

## Direct formate fuel cells: A review

L. An<sup>a\*</sup> and R. Chen<sup>b,c\*</sup>

<sup>a</sup> Department of Mechanical Engineering, The Hong Kong Polytechnic University,  
Hung Hom, Kowloon, Hong Kong SAR, China

<sup>b</sup> Key Laboratory of Low-grade Energy Utilization Technologies and Systems  
(Chongqing University), Ministry of Education, Chongqing 400030, China

<sup>c</sup> Institute of Engineering Thermophysics, Chongqing University, Chongqing 400030,  
China

\*Corresponding authors.

<sup>a</sup> Tel.: 852-27667820; fax: 852-23654703; e-mail: [liang.an@polyu.edu.hk](mailto:liang.an@polyu.edu.hk) (L. An)

<sup>b,c</sup> Tel.: 86-23-65102474; fax: 86-23-65102474; e-mail: [rchen@cqu.edu.cn](mailto:rchen@cqu.edu.cn) (R. Chen)

### Abstract

Direct formate fuel cells (DFFC), which convert the chemical energy stored in formate directly into electricity, are recently attracting more attention, primarily because of the use of the carbon-neutral fuel and the low-cost electrocatalytic and membrane materials. As an emerging energy technology, the DFFC has made a rapid progress in recent years (currently, the state-of-the-art power density is  $591 \text{ mW cm}^{-2}$  at  $60^\circ\text{C}$ ). This article provides a review of past research on the development of this

type of fuel cell, including the working principle, mechanisms and materials of the electrocatalytic oxidation of formate, single-cell designs and performance, as well as innovative system designs. In addition, future perspectives with regard to the development of this fuel cell system are also highlighted.

**Keywords:** Fuel cells; direct formate fuel cells; electrocatalytic mechanisms; electrocatalysts; system designs; cell performance

## 1. Introduction

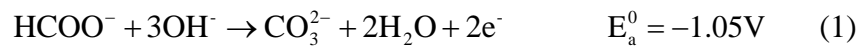
Direct liquid fuel cells (DLFC), which promise to be a clean and efficient energy production technology, have recently attracted worldwide attention, primarily because liquid fuels possess obvious advantages over hydrogen in terms of transportation, storage, as well as handling [1-10]. Among various liquid fuels, formate has recently received ever-increasing attention [11-16], primarily because of several advantageous characteristics in comparison to other fuels: (1) formate is a carbon-neutral fuel that can be easily derived from the reduction of carbon dioxide via artificial photosynthesis [11, 12]; (2) formate oxidation is facile in alkaline media, particularly on the palladium (Pd) [13]; (3) the fuel cell running on formate has a theoretical potential of as high as 1.45 V (air/oxygen as oxidant), which is 0.24 V and 0.31 V higher than the fuel cells running on methanol and ethanol, respectively [14]; (4) unlike in acid media, there is no poisoning effect for the formate oxidation in alkaline media [15]; and (5) formate salts are readily stored, transported, and handled in their solid state and can be easily dissolved into water to form a liquid fuel [16]. For these reasons, many efforts have been devoted to developing direct formate fuel cells (DFFC) and significant progress has been made [17-21]. In addition, formate has also been evaluated as an energy carrier in an electrochemical energy-storage system [22].

The objective of this review is to introduce the physical and chemical processes in this

fuel cell system, summarize recent advances and developments on this type of fuel cell, as well as provide an outlook for future research directions.

## 2. General description of physical and chemical processes

Fig. 1 shows a typical DFFC structure that is composed of an anode and a cathode separated by an anion exchange membrane (AEM). On the anode, the fuel solution (typically, formate salts and alkali are dissolved in the water) flowing into the anode flow channel is transported through the anode diffusion layer (DL) to the anode catalyst layer (CL), where formate ions will be oxidized to generate electrons, water, and carbonate ions according to [13]:

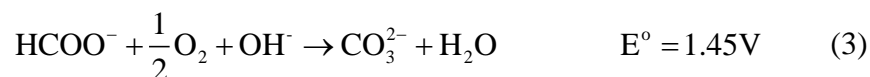


The water in the fuel solution, along with that produced from the formate oxidation reaction (FOR), diffuses through the AEM to the cathode CL, while the produced electrons pass through an external electrical load to the cathode. On the cathode, the oxygen provided by the cathode flow field is transported through the cathode DL to the cathode CL, where oxygen reduction reaction (ORR) takes place to produce hydroxide ions according to [23, 24]:



Subsequently, the generated hydroxide ions are conducted through the AEM to the anode for the FOR. Combining the FOR given by Eq. (1) and the ORR given by Eq.

(2) results in an overall reaction for this fuel cell system:



This theoretical voltage shows an increase as compared with that of fuel cells running methanol (1.23 V) and ethanol (1.14 V) [25, 26].

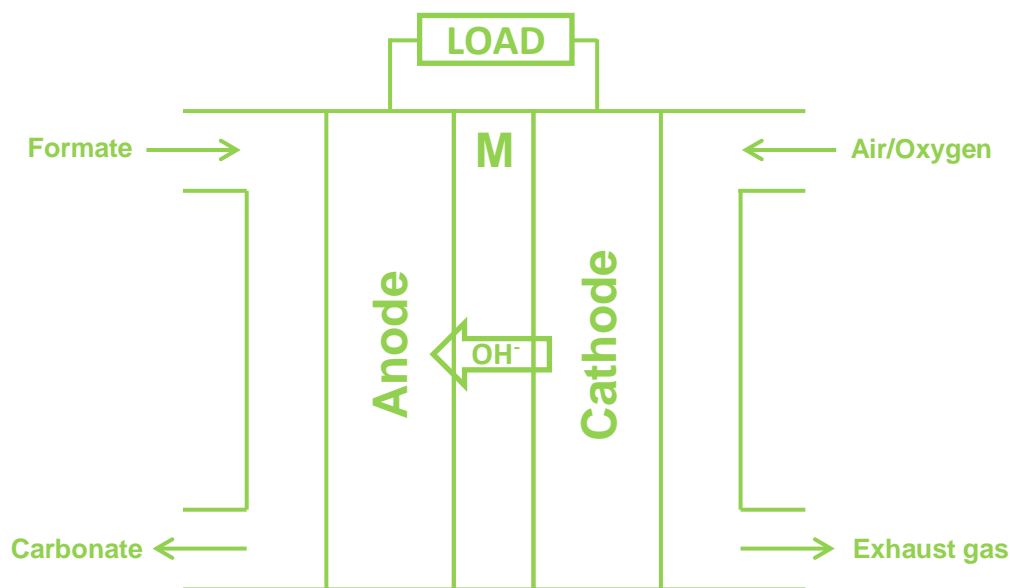


Fig. 1 Schematic of a typical direct formate fuel cell (DFFC).

### 3. Electrocatalytic oxidation of formate

#### 3.1. Mechanisms

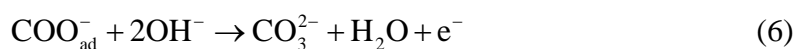
Shedding light on the electrocatalytic mechanism of formate on a certain catalyst will improve our understandings on formate oxidation, which definitely promotes the development of the high-activity catalysts toward formate oxidation. As compared to extensive studies of formic acid oxidation in acid media [27, 28], formate oxidation in alkaline media has not received much attention yet, only few works focusing on Pd [29, 30] and platinum (Pt) [30-35].

### 3.1.1. Palladium

Takamura et al. studied electrocatalytic oxidation of formate on Pd via potential-sweep and galvanostatic methods [29]. They suggested that formate adsorbed on the Pd surface was decomposed into two fragments, such as  $H_{ad}$  and  $COO_{ad}^-$ , according to:



Then,



The net reaction of anodic oxidation of formate is described as in Eq. (1). They also showed that the electrocatalytic oxidation of formate did not involve a strongly bound poisoning intermediate on the Pd surface.

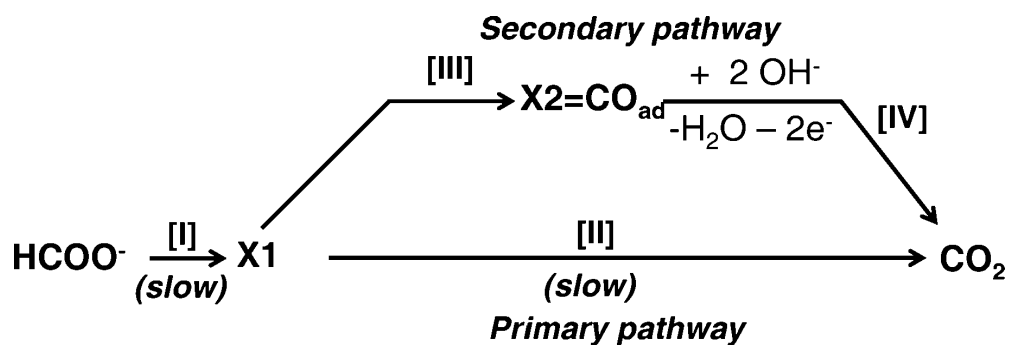
### 3.1.2. Platinum

John et al. [31] studied the mechanism of the formate oxidation on the polycrystalline Pt in highly basic medium ( $pH = 14$ ) via cyclic voltammetry (CV), differential electrochemical mass spectrometry, potential step-linear sweep voltammetry, as well as adsorbate stripping experiments. The results indicated that electrocatalytic oxidation of formate on the polycrystalline Pt was slightly active. In addition, they proposed a dual-pathway mechanism for the formate oxidation on the Pt surface, as shown in Fig. 2a, which is analogous to formic acid oxidation in acid media [32]. In Fig. 2a, X1 stands for the adsorbate for both the primary and secondary

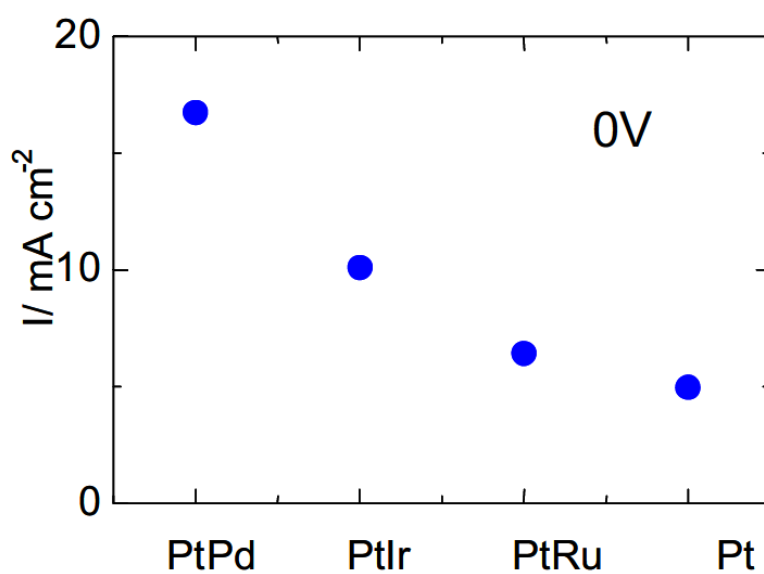
pathways of the formate oxidation, which could either be oxidized to  $\text{CO}_2$  (the primary pathway), or converted to  $\text{CO}_{\text{ad}}$  and its further oxidation to  $\text{CO}_2$  at higher potentials (the secondary pathway). Jiang et al. [33] studied the electrocatalytic oxidation of formate on the Pt black in alkaline media via CV and stripping voltammetry, and then proposed a triple-pathway mechanism. Similar to the dual-pathway mechanism, the active adsorbate was responsible for a direct pathway involving the formate oxidation to  $\text{CO}_2$ , and an indirect pathway involving the formation of  $\text{CO}_{\text{ad}}$  and its further oxidation to  $\text{CO}_2$ . Different from the dual-pathway mechanism, they proposed an independent third pathway via oxidation of less-active adsorbate to  $\text{CO}_2$ . In addition, it was found that all the oxidation reactions involved in the triple pathways were accelerated by increasing the temperature. Christensen et al. [34] studied the formate oxidation on the polycrystalline Pt in alkaline media via in-situ FTIR. It was indicated that adsorbed hydroxyl species had a major effect on steering the reaction mechanism and participating in the oxidation of intermediates. It was also found that the presence of adsorbed hydroxyl species prevented part of the surface from being blocked by adsorbed spectator species such as  $\text{CO}_{\text{ad}}$  and facilitated the adsorption of active O-bonded species. Previdello et al. [35] investigated the electrocatalytic oxidation of formate on the polycrystalline Pt in the presence of different alkali metal cations via CV and chronoamperometry, including  $\text{K}^+$ ,  $\text{Na}^+$  and

$\text{Li}^+$ . Their results showed that the activity towards the formate oxidation was increased in the following sequence:  $\text{Li}^+ < \text{Na}^+ < \text{K}^+$ . It was attributed to the surface blockage rendered by non-covalent interactions between hydrated alkali metal cations and adsorbed oxygenated species on the Pt surface. Taberner et al. [30] investigated the effect of the electrolyte composition on the formate oxidation in a formate-air fuel cell, using  $\text{KCOOH} + \text{KOH}/\text{NaOH}$  as fuel and the air as oxidant. The formate-air fuel cells were comprised of Pd/Pt (9:1) activated sintered nickel anodes and carbon cathodes. They also investigated the effect of the presence of carbonate on the anodic rate of the formate oxidation. Their findings included that (1) at below  $25 \text{ mA cm}^{-2}$ , an increase in the carbonate concentration resulted in a positive effect on the cell voltage; (2) the cathode overpotential was increased with the presence of carbonate, but this negative effect was compensated by its positive effect on the anode; and (3) at  $25 \text{ mA cm}^{-2}$ , the supporting electrolyte change from KOH to NaOH increased the overpotential by about 75 mV [30]. As listed in Table 1, the exchange current densities at various electrolyte compositions were also given by measuring anodic Tafel plots in a half cell. It is seen that the presence of carbonate increases the exchange current density of the formate oxidation. In addition, it was found that the formate oxidation was essentially catalyzed by Pd; while the improvement of the current-potential curves with an addition of carbonate was due to the catalytic effect

by Pt.



(a)



(b)

Fig. 2 (a) Current densities for various catalysts (Pt-Pd, Pt-Ir, Pt-Ru, Pt) in 0.1 M HCOONH<sub>4</sub> at 0 V of CVs [39] and (b) proposed mechanism for the formate oxidation on Pt [31].

In summary, these previous studies show that the electrocatalytic oxidation of formate on Pt in alkaline media occurs to a significantly lower extent as compared to formic acid in acidic media.

### 3.2. Electrocatalysts

### 3.2.1. Pt and Pt-based electrocatalysts

It is the fact that the electrocatalytic activity of the formate oxidation on Pt is much lower than that on Pd. For this reason, only few studies have been done using Pt and Pt-based catalysts as the electrocatalytic materials for the formate oxidation in alkaline media [36-39]. Rosenbaum et al. [36] investigated the formate oxidation on platinum black modified electrodes under microbial fuel cell conditions (at neutral pH, at room temperature and in microbial culture solutions) via CV, chronoamperometry, as well as potentiostatic coulometry. The experimental results showed that the current densities of the formate oxidation were up to  $6 \text{ mA cm}^{-2}$  at an oxidation potential of 0.2 V, and a coulombic efficiency was 97%. Under the same condition, the kinetics of the electrocatalytic oxidation of formate was found to be significantly higher (ten-fold) than the ethanol oxidation did. Ohyama et al. [37, 38] developed a fuel cell using ammonium formate as fuel and investigated electrocatalytic activity of ammonium formate on Pt and Pt-iridium (Ir) via CV. It was found that the Pt-Ir catalysts could effectively oxidize ammonium formate, as they could effectively oxidize CO layer to  $\text{CO}_2$ . In addition, Aoki et al. [39] investigated the Pt-Pd catalysts for the electrocatalytic oxidation of ammonia formate via CV. Similarly, it was also found that the Pt-Pd catalysts can effectively oxidize ammonium formate. To further confirm this result, they conducted linear sweep voltammetric measurement ( $1 \text{ mVs}^{-1}$ ) and

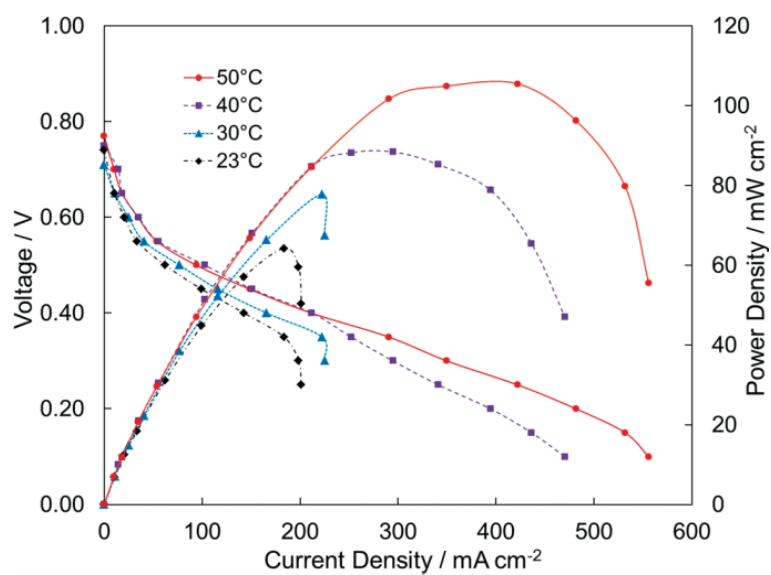
found that the current density peak of the Pt-Pd catalysts was higher than that of the Pt catalysts. They also showed that among various catalysts (Pt, Pt-Ir, Pt-Pd, Pt-Ru), the Pt-Pd catalysts resulted in the highest current density for the electrocatalytic oxidation of ammonium formate (0.1 M), as presented in Fig. 2b.

### **3.2.2. Pd and Pd-based electrocatalysts**

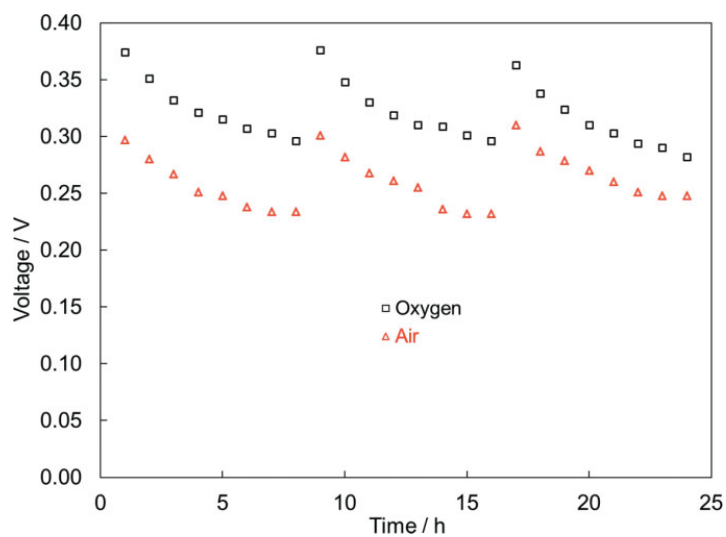
As mentioned earlier, the electrocatalytic activity of formate oxidation on Pd is much higher than that on Pt. As a result, Pd and Pd-based catalysts are extensively used as the electrocatalytic materials for formate oxidation [40-42]. Bartrom et al. [40] investigated the Pd catalysts for the electrocatalytic oxidation of formate in alkaline media. It was shown that unlike the Pt catalysts, formate could be oxidized rather efficiently and there was no strongly-bound intermediate on the Pd surface. They demonstrated that using the Pd catalysts enabled this type of fuel cell to operate with the air or even without supporting electrolyte such as KOH. It should be pointed out that other liquid fuels, such as ethanol, have to be mixed with the alkali in the fuel solution to achieve the high performance [8, 9]. In addition, they also studied the effect of the formate salt type (HCOOK/HCOONa) on the cell performance, and showed that the peak power density of the fuel cell running on HCOOK was 144 mW cm<sup>-2</sup>, while the fuel cell running on HCOONa resulted in a peak power density of 125 mW cm<sup>-2</sup> at 60°C. Attempts have also been made to combine Pd with other metal,

such as Au and Cu, to improve catalytic activity for formate oxidation in alkaline media [13, 41-43]. Noborikawa et al. [41] synthesized the Pd-Cu/C alloy and Pd/C catalysts via metal salt reduction with sodium hypophosphite. As compared to Pd/C, the kinetics of the formate oxidation in alkaline media was enhanced by using the Pd-Cu/C alloy. It is attributed to the fact that an addition of Cu to Pd induces an electronic effect on the Pd surface: charge transfer from Pd to Cu, which plays an important role in the formate oxidation. Also, the Pd-Cu/C alloy catalysts showed a high activity toward not only the formate oxidation, but also the oxidation of other fuels in alkaline media, such as ethanol and ethylene glycol [41, 43]. Silva et al. [42] prepared the Pd-Au/C catalysts in different atomic ratios (90:10, 80:20, 70:30, and 50:50) via metal salt reduction with sodium borohydride for the electrocatalytic oxidation of formate in alkaline media. They showed that the mean particle size of the Pd-Au/C catalysts were between 4 nm and 10 nm. They also found that the use of Pd-Au/C catalysts (90:10 and 80:20) in DFFCs resulted in about 15 % higher in the peak power density than the Pd/C catalysts did. Li et al. [13] prepared a 3-D Pd-Au/Ni foam porous electrode for the formate oxidation via a binder-free spontaneous-deposition method. It was found that the PdAu/Ni foam electrode shows a better catalytic activity than Pd/Ni foam electrode. The enhanced electrocatalytic activity on PdAu/Ni foam electrode was attributed to the so-called electronic effect.

In summary, the discussion has been focused on two types of electrocatalyst, i.e., Pt/Pt-based and Pd/Pd-based electrocatalysts. In the future, non-precious metals should also be considered as a good candidate for electrocatalysts toward formate oxidation in alkaline media.



(a)



(b)

Fig. 3 The DFFC performance evaluation: (a) voltage/power-current curves and (b) constant-current discharging behaviors [49].

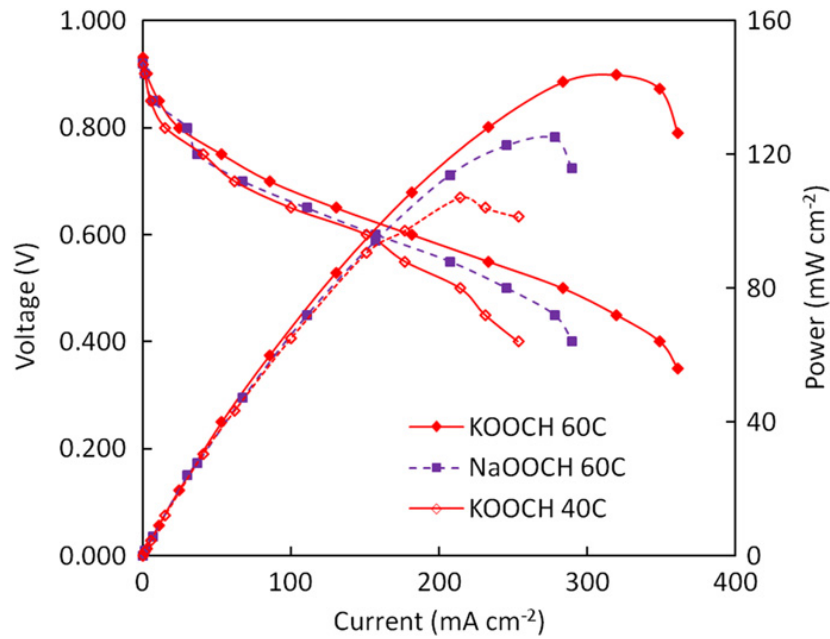
#### 4. Single-cell designs and performance

The fuel cell performance depends on not only the electrocatalytic and membrane materials [44, 45], but also the structural design parameters that determine the transport rates of mass, ions and electrons through the fuel cell structure [46], as well as the operating parameters that directly link to the fuel cell power output [47]. As summarized in Tables 2 and 3, it can be seen that although the DFFC is still an emerging energy technology, the power density has been substantially boosted from  $\sim 50 \text{ mW cm}^{-2}$  to  $591 \text{ mW cm}^{-2}$  in recent years. For example, Jiang et al. [48] fabricated a  $5.0 \text{ cm}^2$  DFFC using Pd/C ( $4.0 \text{ mg cm}^{-2}$ ) and Ag/C ( $8.0 \text{ mg cm}^{-2}$ ) as anode and cathode catalysts, respectively, as well as a  $40\text{-}\mu\text{m}$  polybenzimidazole-based membrane. The fuel cell was evaluated at temperatures ranging from  $80^\circ\text{C}$  to  $120^\circ\text{C}$  with the fuel solution containing HCOOK and  $2.0 \text{ M}$  KOH fed at a flow rate of  $6.0 \text{ mL min}^{-1}$  and pure oxygen as oxidant at a flow rate of  $200 \text{ sccm}$ . The highest power density of about  $160 \text{ mW cm}^{-2}$  was achieved with  $6.0 \text{ M}$  HCOOK in the fuel solution at  $120^\circ\text{C}$ . It was also shown from CV results that the kinetics of the formate oxidation on Pd in alkaline media was substantially enhanced with the temperature. Nguyen et al. [49] developed a DFFC that can run without an added alkali at low temperatures. As shown in Fig. 3a, it was demonstrated that the fuel cell using  $1 \text{ M}$  HCOOK as fuel and pure oxygen as oxidant resulted in a peak

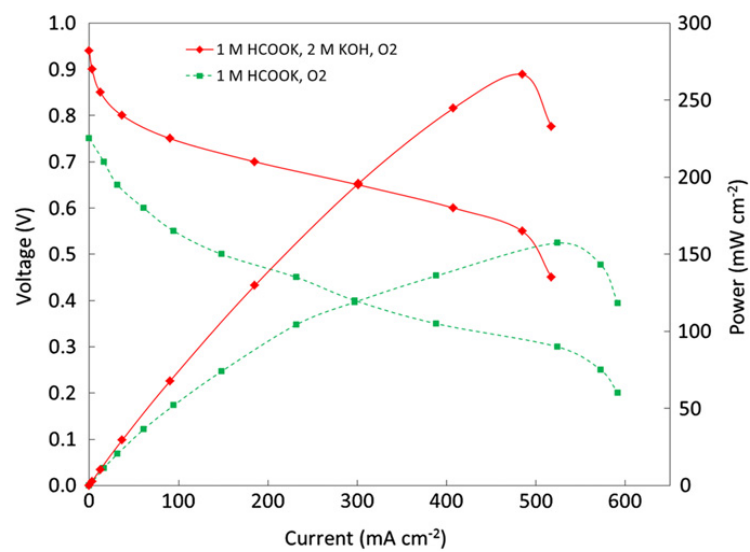
power density of  $64 \text{ mW cm}^{-2}$  and  $106 \text{ mW cm}^{-2}$ , respectively, at  $23^\circ\text{C}$  and  $50^\circ\text{C}$ . In addition, the change of the oxidant from pure oxygen to the air resulted in a peak power density of  $27 \text{ mW cm}^{-2}$  and  $76 \text{ mW cm}^{-2}$ , respectively, at  $23^\circ\text{C}$  and  $50^\circ\text{C}$ . They also investigated the constant-current discharging behaviors and found that the cell voltage suffered a gradual decay, but it could be recovered, as shown in Fig. 3b. Furthermore, it was indicated from the electrochemical analysis that the formate oxidation was not dependent of pH ranging between 9 and 14, which is the reason that the DFFC can run without the addition of an alkali to the fuel solution. Bartrom et al. [50, 51] fabricated a high-performance DFFC employing the Pd ( $2.0 \text{ mg cm}^{-2}$ ) and Pt ( $2.0 \text{ mg cm}^{-2}$ ) catalysts at the anode and cathode, respectively, as well as an AEM (Tokuyama A201). The effects of the operating parameters on the cell performance were investigated, including the fuel salt type (HCOOK/HCOONa), the oxidant type (air/oxygen), the formate concentration (HCOOK: 1 M, 2 M, 3M), the alkali concentration (KOH: 0 M, 1 M, 2 M), and the operating temperature ( $40^\circ\text{C}/60^\circ\text{C}$ ). By doing so, it was demonstrated that the fuel cell resulted in an open-circuit voltage (OCV) of 0.931 and a peak power density of  $144 \text{ mW cm}^{-2}$  when operated at  $60^\circ\text{C}$  using 1.0 M HCOOK and 2.0 M KOH as fuel and pure oxygen as oxidant, as shown in Fig. 4a. They further improved the DFFC performance by optimizing the preparation method of the anode CL and the corresponding catalyst loading [52]. It

was suggested that an optimal anode was obtained by a combination of spray painting on the membrane and brush painting on the DL. After that, the effects of the above-mentioned operating parameters were investigated again to maximize the power output. As shown in Fig. 4b, it was demonstrated that the peak power density reached  $267 \text{ mW cm}^{-2}$  when operated at  $60^\circ\text{C}$  with  $1 \text{ M HCOOK} + 2 \text{ M KOH}$  as fuel and pure oxygen as oxidant; decreased to  $157 \text{ mW cm}^{-2}$  when the supporting electrolyte (KOH) was removed from the fuel solution; and further decreased to  $105 \text{ mW cm}^{-2}$  when the oxidant was changed to the air. It is interesting to note that this fuel cell structure can run not only on formate, but also on other liquid fuels, as presented in Fig. 4c, such as ethanol and ethylene glycol [53]. Recently, Nguyen et al. [54] fabricated and tested a Pt-free DFFC employing the Pd black catalysts at the anode, the commercial Fe-Co catalysts (ACTA Hypermec<sup>TM</sup> 4020) at the cathode, as well as an AEM (Tokuyama A201). The performance tests showed that the fuel cell resulted in a peak power density of  $45 \text{ mW cm}^{-2}$  at  $20^\circ\text{C}$  when operated with  $1 \text{ M HCOOK} + 2 \text{ M KOH}$  as fuel and pure oxygen as oxidant. In addition, using the air decreased the peak power density to  $35 \text{ mW cm}^{-2}$  and further to  $18 \text{ mW cm}^{-2}$  when the supporting electrolyte was removed from the fuel solution. Zeng et al. [55] developed and tested a single DFFC that consists of a Pd/C catalyst at the anode, a quaternized polysulfone membrane, and a non-precious Fe-Co catalyst at the cathode. It was

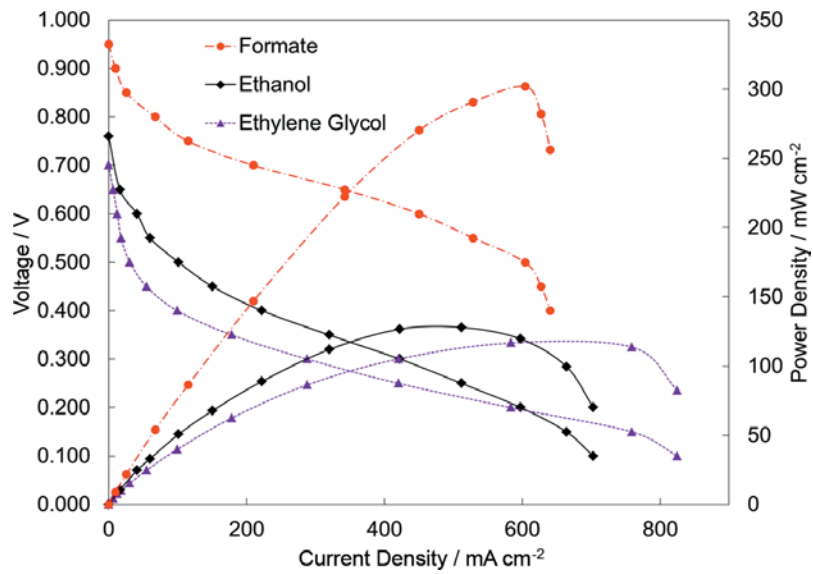
shown that operating the fuel cell at 80°C resulted in a peak power density of 250 mW cm<sup>-2</sup> and 130 mW cm<sup>-2</sup>, respectively, with and without addition of an alkali. In addition, it was found that there was no significant decay in the cell voltage when operated at 60°C with a current density of 100 mA cm<sup>-2</sup> for about 134 h.



(a)



(b)



(c)

Fig. 4 The DFFC performance improvements through optimizing (a) the operating parameters [50] and (b) the structural design parameters [52]; and (c) performance comparison among fuel cells running on various fuels (formate, ethanol, ethylene glycol) [52].

In summary, the DFFC performance with various electrocatalytic materials, structural design parameters, as well as operating parameters has been summarized and discussed. The fuel cell, fabricated with the Pd anode catalysts, an AEM (Tokuyama A201), and Pt cathode catalysts and operated with the fuel-electrolyte-fed mode, results in the highest power density. In the future, particular attention should also be paid to understand the mechanisms and characteristics of species transport through the fuel cell structure and then to design new electrodes that enable high transport rates of mass, ions and electrons.

## 5. Innovative system designs

In addition to the convention formate fuel cells, recently, there are some new types of fuel cell running on formate, including formate-hydrogen peroxide fuel cells [13, 56, 57], membraneless formate fuel cells [15, 58], microfluidic fuel cells [16, 59, 60], as well as an electrochemical energy-storage device using formate as energy carrier [22].

### 5.1. Formate-hydrogen peroxide fuel cells

Li et al. [13] proposed a formate-hydrogen peroxide fuel cell that is composed of an alkaline anode, a cation exchange membrane (CEM), and an acid cathode, as shown in Fig. 5a. On the anode, formate ions react with hydroxide ions to generate electrons, water and carbonate ions according to Eq. (1). The released electrons travel through the external circuit to the cathode. On the cathode, hydrogen peroxide reacts with protons and electrons to produce water according to [61]:

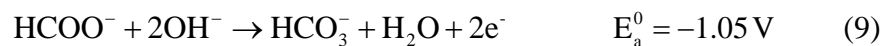


In the meantime, sodium ions as charge carrier will penetrate through the membrane to the cathode. Hence, the overall reaction in this type of fuel cell is:



It is seen that the theoretical voltage can reach 2.83 V, which is 1.38 V higher than the conventional DFFCs using air/oxygen as oxidant [14]. The membrane electrode

assembly (MEA) was comprised of two Pd-Au/Ni foam electrodes and a pre-treated Nafion 115 membrane. The performance tests showed that the fuel cell resulted in an OCV of 1.51 V, a peak power density of 331 mW cm<sup>-2</sup>, and a maximum current density of 924 mA cm<sup>-2</sup> at 60°C, which are much higher than those achieved by the conventional DFFCs operated with air/oxygen. In addition, Li et al. [56] investigated effects of the structural design and operating parameters to further improve the cell performance, including catalyst loadings at two electrodes, the operating temperature, the formate concentration, as well as the sodium hydroxide concentration. As shown in Fig. 5b, it was shown that the use of the optimal electrode design (Pd loading in the anode CL is 2.0 mg cm<sup>-2</sup> and Pt loading in the cathode CL is 2.0 mg cm<sup>-2</sup>) and the optimal solution composition (1.0 M HCOONa + 3.0 M NaOH) resulted in a peak power density of 591 mW cm<sup>-2</sup> at 60°C. Recently, Li et al. [57] fabricated and tested a liquid-electrolyte-free DFFC using hydrogen peroxide as oxidant. On the anode, as a result of no addition of an alkali to the fuel solution, formate reacts with hydroxide ions to possibly generate electrons, water and bicarbonate ions according to [57]:



On the cathode, hydrogen peroxide reduction reaction will take place in alkaline media according to [24]:

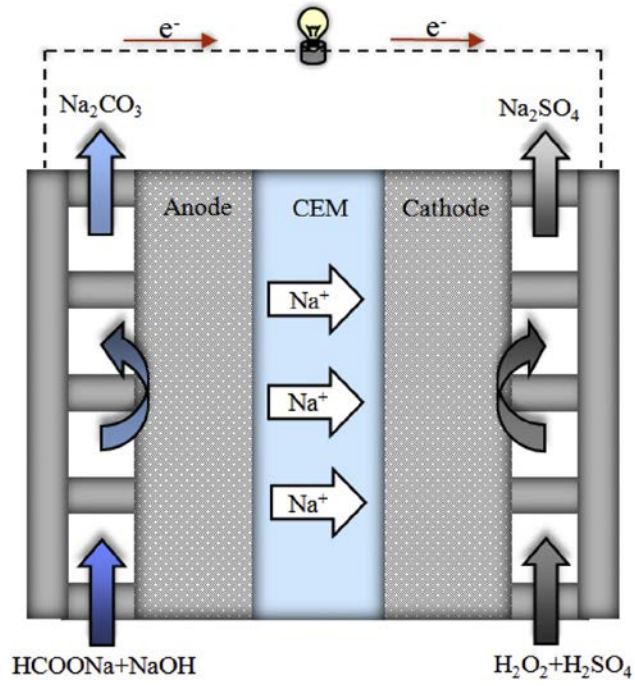


The produced hydroxide ions will migrate through the AEM to anode for the FOR.

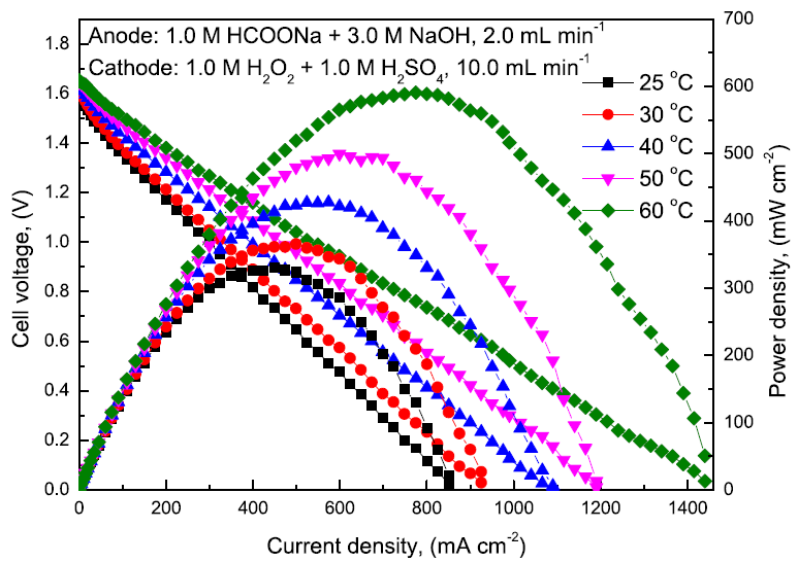
Hence, the overall reaction for this type of fuel cell is:



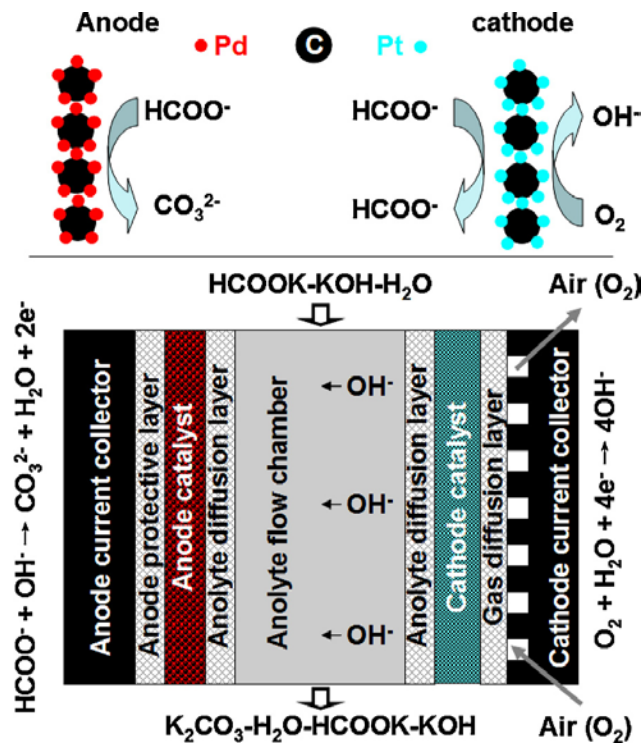
It is shown that theoretically, the voltage of this fuel cell can reach 1.92 V, which is 0.47 V higher than that using air/oxygen as oxidant. The MEA was comprised of a Pd/C-based anode (2.0 mg cm<sup>-2</sup>), a Pt/C-based cathode (2.0 mg cm<sup>-2</sup>), as well as an AEM (Tokuyama A201). The performance evaluation was conducted at 40°C with a 1.0-M formate aqueous solution (without an alkali) at a flow rate of 1.0 mL min<sup>-1</sup> and a 15 wt. % hydrogen peroxide aqueous solution (without an acid) at a flow rate of 3.0 mL min<sup>-1</sup>. It was shown that this liquid-electrolyte-free fuel cell led to a peak power density of 23 mW cm<sup>-2</sup> and a maximum current density of 180 mA cm<sup>-2</sup>. In summary, there is still plenty of room to boost the cell performance, due to the large difference between actual and theoretical voltages. It should be pointed out that hydrogen peroxide is not stable chemically and electrochemically, particularly in alkaline media, decomposing into water and oxygen and thus forming two-phase counterflow [46]. The rate of hydrogen peroxide decomposition can be reduced by optimizing the pH value, the hydrogen peroxide concentration, the temperature of the aqueous solution, and the electrochemical properties of electrode materials [62]. Hence, the issue associated with hydrogen peroxide decomposition should be addressed in the future.



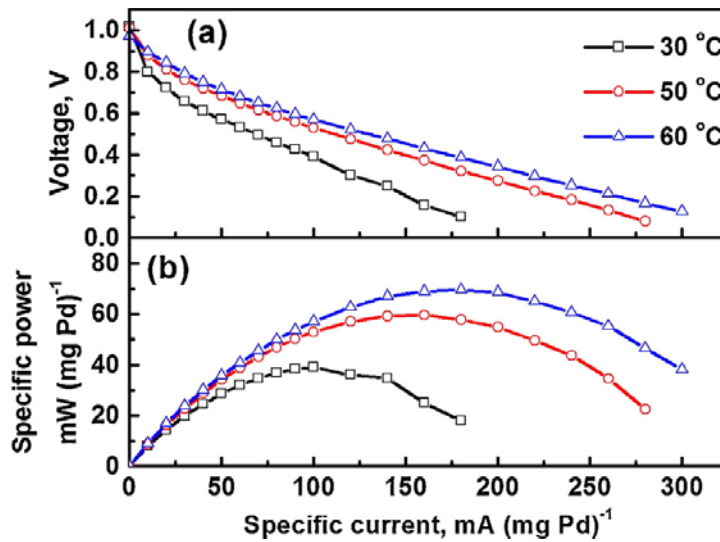
(a)



(b)



(c)



(d)

Fig. 5 A formate-hydrogen peroxide fuel cell: (a) schematic [13] and (b) performance

[56]. A membraneless formate fuel cell: (c) schematic and (d) performance [15].

## 5.2. Membraneless formate fuel cells

Yu et al. [15] proposed a membraneless DFFC using highly selective electrocatalysts, which is simpler than conventional membraneless fuel cells achieved by non-mixing laminar flows. Specifically, Pd/C ( $1.0 \text{ mg cm}^{-2}$ ) and Pt/C ( $1.0 \text{ mg cm}^{-2}$ ) were used as anode and cathode catalysts, respectively. As mentioned earlier, Pt is weakly active to the formate oxidation in alkaline media so that electrocatalytic oxidation of formate will not take place on the cathode [31]. The fuel solution containing HCOOK and KOH was fed through a chamber between the anode and cathode CLs. The fuel solution flowing through the chamber not only sustains the migration of hydroxide ions, but also delivers reactants to the anode CL. As illustrated in Fig. 5c, a membraneless DFFC was fabricated with an active area of  $5 \text{ cm}^2$  and a 2-mm-thick flow chamber. The performance evaluation was conducted when the cell was operated with a fuel solution containing 2.0 M HCOOK and 2.0 M KOH flowing through the chamber at a flow rate of  $0.5 \text{ mL min}^{-1}$  and pure oxygen fed to the cathode flow channel at a flow rate of 100 sccm. It was demonstrated from Fig. 5d that this membraneless fuel cell yielded an OCV of about 1.1 V and a specific power of about  $75 \text{ mW (mg Pd)}^{-1}$  at  $60^\circ\text{C}$ . Recently, they used  $\text{MnNiCoO}_4/\text{N-MWCNT}$  to replace Pt/C as cathode catalysts in membraneless formate fuel cells [58]. It was found that the cell could result in an OCV of 1.05 V and a specific power density of

about  $90 \text{ mW cm}^{-2}$  at  $50^\circ\text{C}$ . In summary, using a flow chamber in fuel cells indeed avoids the need for inefficient and costly AEMs, simplifies the cell configuration, as well as lowers the system cost, but limits the power output due to the large gap between two electrodes.

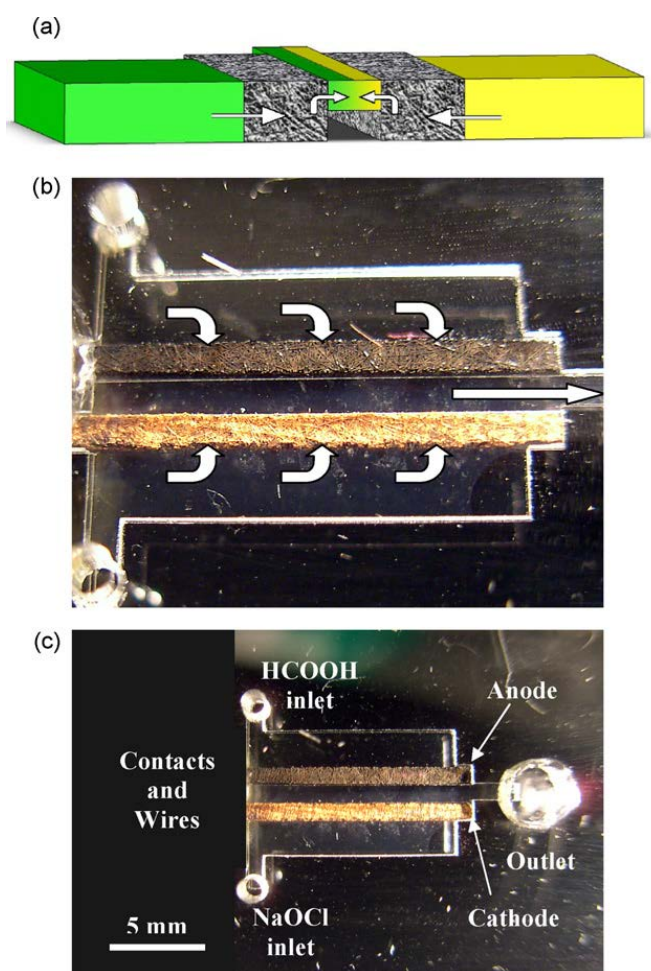
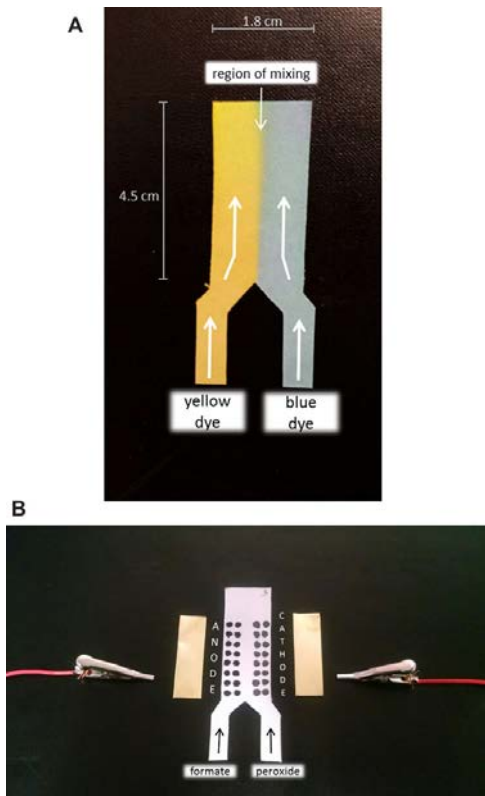


Fig. 6 A microfluidic formate fuel cell with flow-through porous electrodes: (a) schematic, (b) image of the assembled cell with porous palladium and gold electrodes, and (c) the labeled image of the assembled cell [16].

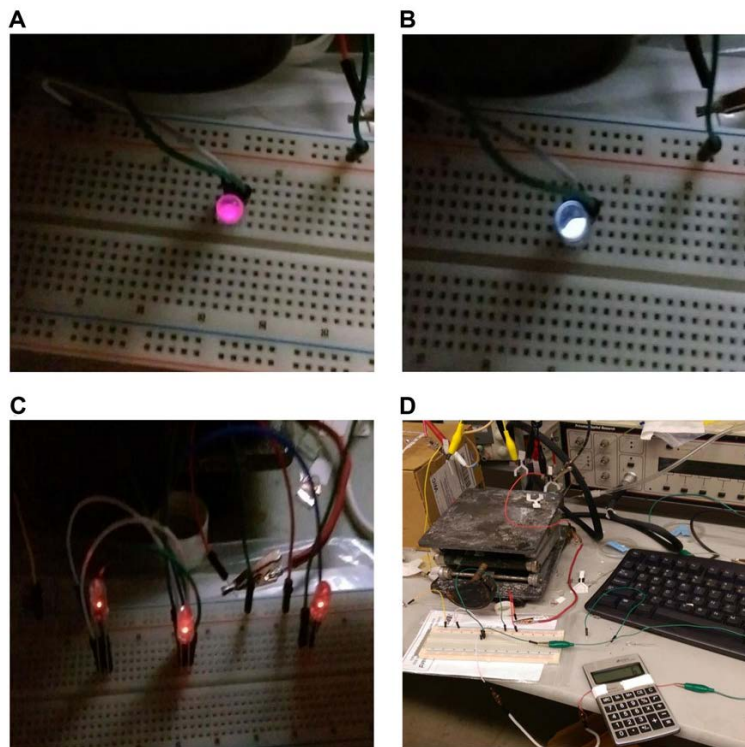
### 5.3. Microfluidic formate fuel cells

Kjeang et al. [16] developed an alkaline microfluidic fuel cell running on sodium formate as fuel and sodium hypochlorite as oxidant, in which Pd and Au were electrodeposited on porous carbon paper substrates as the anode and cathode, respectively, as shown in Fig. 6. This microfluidic formate fuel cell with flow-through porous electrodes was operated with the anolyte (1.2 M formate + 1.6 M NaOH) and catholyte (0.67 M hypochlorite + 2.8 M NaOH) at flow rates ranging from 2.0  $\mu\text{L min}^{-1}$  to 300.0  $\mu\text{L min}^{-1}$ . The fuel cell exhibited stable co-laminar flows without any gas evolution or other disturbances, and the OCV was steady between 1.37 V and 1.42 V. It was also demonstrated that a peak power density up to 52  $\text{mW cm}^{-2}$  and an overall energy-conversion efficiency up to 30% at room temperature. This microfluidic fuel cell concurrently achieved high power densities and fuel utilization, thereby enabling a high overall energy-conversion efficiency. In addition, it was inferred that the performance would be further enhanced by optimizing the fuel cell structure and developing high-activity electrocatalysts. Recently, Copenhaver et al. [59] fabricated a paper microfluidic fuel cell running on formate as fuel and hydrogen peroxide as oxidant. As shown in Fig. 7a, this fuel cell was created by using a typical Y-shaped design, in which co-laminar flow was realized as the fuel and oxidant traveled upwards driven by the capillary action. Like a membraneless laminar flow

fuel cell, there is no physical membrane barrier placed between two streams. The effect of the electrolyte composition on the performance was investigated, including the HCOOK concentration, the KOH concentration, as well as the H<sub>2</sub>O<sub>2</sub> concentration. It was found that the optimal concentrations of HCOOK and H<sub>2</sub>O<sub>2</sub> were 5.0 M and 30 wt. % H<sub>2</sub>O<sub>2</sub>, respectively, while the effect of adding KOH was insignificant. By doing so, it was showed that two cells in both series and parallel configurations resulted in a peak power density of around 2.5 mW (mg Pd)<sup>-1</sup>, while, two cells yielded an OCV of about 1.05 V in a series configuration and about 0.6 V in a parallel configuration, respectively. Further, they optimized the structural design and operating parameters, including the lateral column dimension, the current collector, and the cathode composition [60]. By doing so, it was found that a peak power density of 2.53 mW cm<sup>-2</sup> was achieved when fabricated: (1) with inlets of width and length of 0.5 cm and 1.0 cm, respectively, and the lateral column of a width and length of 1.0 cm and 3.0 cm, respectively; (2) with a 5 wt. % mass of carbon to paint cathode electrode; and (3) with steel mesh as current collectors. It can be seen from Fig. 7b that the two cells in a series configuration could power light-emitting diodes or a handheld calculator. In addition, the microfluidic formate fuel cell also has potential applications in point-of-care diagnostic devices and other electrochemical sensors.



(a)



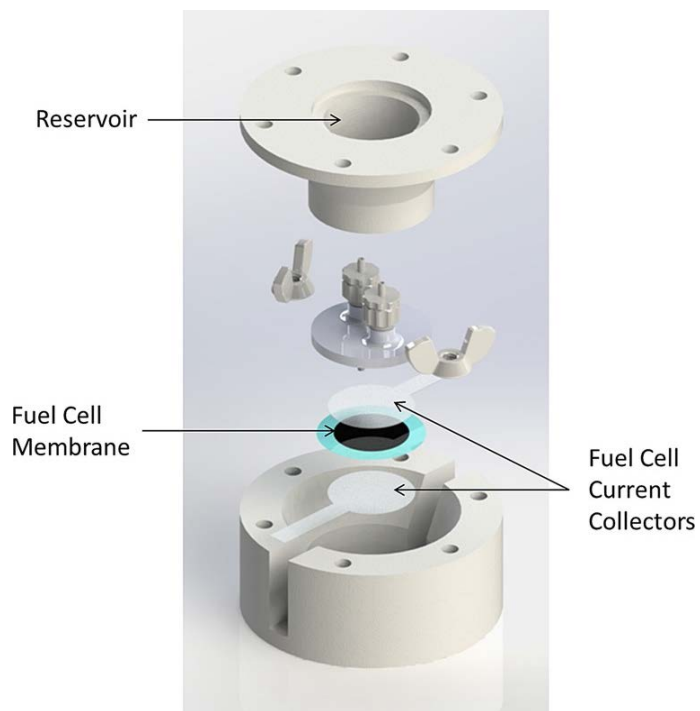
(b)

Fig. 7 A microfluidic formate fuel cell on paper: (a) Y-shaped design [59] and (b) demos (three light-emitting diodes and a handheld calculator) [60].

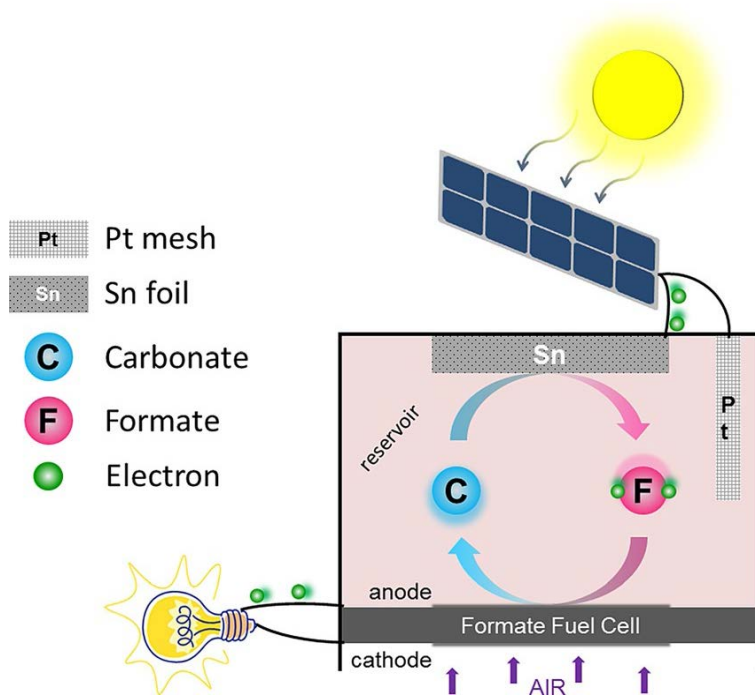
#### **5.4. An energy-storage device using formate as energy carrier**

Formate can be an energy carrier in a renewable energy-storage system via interconversion between formate and carbon dioxide. Recently, Vo et al. [61] proposed an energy-storage device that integrates the electrochemical reduction of carbon dioxide to formate and conversion of formate to energy in the same device, as shown in Fig. 8a, which is analogous to rechargeable batteries [63]. In principle, renewable power, such as solar and wind, can be stored in the formate solution via carbonate-to-formate conversion by the electrochemical reduction of carbonate (i.e., electrolysis mode); and then the power can be released via a carbonate-to-formate conversion by the electrochemical oxidation of formate (i.e., fuel cell mode), as illustrated in Fig. 8b. Since the device was operated completely in a passive mode on the anode and cathode, the peak power density was only  $2.5 \text{ mW cm}^{-2}$  at room temperature [61]. In addition to the electrochemical method with an electrocatalyst, the reduction of carbon dioxide to formate can also be achieved via an electrochemical method with a particular type of enzyme [64], a chemical process [65], as well as a photoelectrochemical approach [66]. In summary, the power of this energy-storage device has to be much improved before the widespread

commercialization becomes possible.



(a)



(b)

Fig. 8 An electrochemical energy-storage system using formate as energy carrier: (a)

schematic and (b) working principle [61].

## **6. Concluding remarks**

As an emerging energy technology, the DFFC has made a rapid progress in recent years. This article provides an overview of past research on the development on direct formate fuel cells. It includes a brief introduction to the physical and chemical processes, electrocatalytic mechanisms of formate oxidation on Pt and Pd surfaces in alkaline media, electrocatalysts toward the formate oxidation, single-cell designs and performance, as well as the innovative system designs. In addition, it is indicated that there is still a plenty of room to improve DFFC performance by developing high-performance, cost-effective membrane and electrocatalytic materials and optimizing the structural design and operating parameters of the fuel cell. Specifically, we need to (1) develop high-conductivity, high-durability, and cost-effective alkaline membranes at elevated temperatures and soluble in certain solvents for use as an ionomer in preparing catalyst layers, (2) synthesize high-activity, high-durability, and non-precious-metal electrocatalysts for formate oxidation in alkaline media, (3) understand the mechanisms and characteristics of species transport through the fuel cell structure, (4) design and optimize the fuel cell structure that enables high transport rates of mass, ions and electrons, and (5) optimize the fuel cell operating parameters that maximize the power output of the fuel cell system.

## **Acknowledgements**

The authors gratefully acknowledge the financial supports of the Natural Science Foundation of China (No. 51506039 and No. 51576021).

## **References**

- [1] E.H. Yu, X. Wang, U. Krewer, L. Lid, K. Scott, Direct oxidation alkaline fuel cells: from materials to systems, *Energy Environ. Sci.* 5 (2012) 5668-5680.
- [2] L. An, T.S. Zhao, J.B. Xu, A bi-functional cathode structure for alkaline-acid direct ethanol fuel cells, *Int. J. Hydrogen Energy* 36 (2011) 13089-13095.
- [3] E. Antolini, E.R. Gonzalez, Alkaline direct alcohol fuel cells, *J. Power Sources* 195 (2010) 3431-3450.
- [4] L. An, T.S. Zhao, S.Y. Shen, Q.X. Wu, R. Chen, An alkaline direct oxidation fuel cell with non-platinum catalysts capable of converting glucose to electricity at high power output, *J. Power Sources* 196 (2011) 186-190.
- [5] L. An, L. Zeng, T.S. Zhao, An alkaline direct ethylene glycol fuel cell with an alkali-doped polybenzimidazole membrane, *Int. J. Hydrogen Energy* 38 (2013) 10602-10606.
- [6] Y.S. Li, Y.L. He, Layer reduction method for fabricating Pd-coated Ni foams as high-performance ethanol electrode for anion-exchange membrane fuel cells, *RSC*

Advances 4 (2014) 16879-16884.

[7] Y.S. Li, Y.L. He, W.W. Yang, Performance characteristics of air-breathing anion-exchange membrane direct ethanol fuel cells, *International Journal of Hydrogen Energy* 38 (2013) 13427-13433.

[8] Y.S. Li, T.S. Zhao, Ultra-low catalyst loading cathode electrode for anion-exchange membrane fuel cells, *International Journal of Hydrogen Energy* 37 (2012) 15334-15338.

[9] L. An, T.S. Zhao, X.L. Zhou, L. Wei, X.H. Yan, A high-performance ethanol-hydrogen peroxide fuel cell, *RSC Advances* 4 (2014) 65031-65034.

[10] L. An, T.S. Zhao, X.L. Zhou, X.H. Yan, C.Y. Jung, A low-cost, high-performance zinc-hydrogen peroxide fuel cell, *J. Power Sources* 275 (2015) 831-834.

[11] X. Cheng, R. Chen, X. Zhu, Q. Liao, X. He, S. Li, L. Li, Optofluidic membrane microreactor for photocatalytic reduction of CO<sub>2</sub>, *Int. J. Hydrogen Energy* 41 (2016) 2457-2465.

[12] L. An, T.S. Zhao, Z.H. Chai, P. Tan, L. Zeng, Mathematical modeling of an anion-exchange membrane water electrolyzer for hydrogen production, *Int. J. Hydrogen Energy* 39 (2014) 19869-19876.

[13] Y.S. Li, Y.L. He, W.W. Yang, A high-performance direct formate-peroxide fuel cell with palladium-gold alloy coated foam electrodes, *Journal of Power Sources* 278

(2015) 569-573.

[14] L. An, T.S. Zhao, S.Y. Shen, Q.X. Wu, R. Chen, Performance of a direct ethylene glycol fuel cell with an anion-exchange membrane, *Int. J. Hydrogen Energy* 35 (2010) 4329-4335.

[15] X.W. Yu, A. Manthiram, Catalyst-selective, scalable membraneless alkaline direct formate fuel cells, *Applied Catalysis B: Environmental* 165 (2015) 63-67.

[16] E. Kjeang, R. Michel, D.A. Harrington, D. Sinton, N. Djilali, An alkaline microfluidic fuel cell based on formate and hypochlorite bleach, *Electrochimica Acta* 54 (2008) 698-705.

[17] J. Joo, T. Uchida, A. Cuesta, M.T.M. Koper, M. Osawa, The effect of pH on the electrocatalytic oxidation of formic acid/formate on platinum: A mechanistic study by surface-enhanced infrared spectroscopy coupled with cyclic voltammetry, *Electrochimica Acta* 129 (2014) 127-136.

[18] L. An, T.S. Zhao, Y.S. Li, Q.X. Wu, Charge carriers in alkaline direct oxidation fuel cells, *Energy & Environmental Science* 5 (2012) 7536-7538.

[19] G.L. Soloveichik, Liquid fuel cells, *Beilstein Journal of Nanotechnology*, 5 (2014) 1399-1418.

[20] L. An, T.S. Zhao, L. Zeng, Agar chemical hydrogel electrode binder for fuel-electrolyte-fed fuel cells, *Applied Energy* 109 (2013) 67-71.

- [21] J. Noborikawa, J. Lau, J. Ta, S. Hu, L. Scudiero, S. Derakhsha, S. Ha, J.L. Haan, Palladium-copper electrocatalyst for promotion of oxidation of formate and ethanol in alkaline media, *Electrochimica Acta* 137 (2014) 654-660.
- [22] T. Vo, K. Purohit, C. Nguyen, B. Biggs, S. Mayoral, J.L. Haan, Formate: an energy storage and transport bridge between carbon dioxide and a formate fuel cell in a single device, *ChemSusChem* 8 (2015) 3853-3858.
- [23] L. An, T.S. Zhao, An alkaline direct ethanol fuel cell with a cation exchange membrane, *Energy Environ. Sci.* 4 (2011) 2213-2217.
- [24] L. An, T.S. Zhao, L. Zeng, X.H. Yan, Performance of an alkaline direct ethanol fuel cell with hydrogen peroxide as oxidant, *Int. J. Hydrogen Energy* 39 (2014) 2320-2324.
- [25] T.S. Zhao, C. Xu, R. Chen, W.W. Yang, Mass transport phenomena in direct methanol fuel cells, *Progress in Energy and Combustion Science* 35 (2009) 275-292.
- [26] L. An, T.S. Zhao, Y.S. Li, Carbon-neutral sustainable energy technology: Direct ethanol fuel cells, *Renewable and Sustainable Energy Reviews* 50 (2015) 1462-1468.
- [27] M. Baldauf, D. M. Kolb, Formic acid oxidation on ultrathin Pd films on Au (hkl) and Pt (hkl) electrodes, *The Journal of Physical Chemistry* 100 (1996) 11375-11381.
- [28] D. Morales-Acosta, J. Ledesma-Garcia, L.A. Godinez, H.G. Rodríguez, L. Alvarez-Contreras, L.G. Arriaga, Development of Pd and Pd-Co catalysts supported

on multi-walled carbon nanotubes for formic acid oxidation, *J. Power Sources* 195 (2010) 461-465.

[29] T. Takamura, F. Mochimaru, Adsorption and oxidation of formate on palladium in alkaline solution, *Electrochimica Acta* 14 (1969) 111-119.

[30] P. Taberner, J. Hettbaum, W. Vielstich, The influence of the electrolyte composition on the formate oxidation in alkaline formate-air fuel cells, *Electrochimica Acta* 21 (1976) 439-440.

[31] J. John, H. Wang, E.D. Rus, H.D. Abruña, Mechanistic studies of formate oxidation on platinum in alkaline medium, *J. Phys. Chem. C* 116 (2012) 5810–5820.

[32] S.G. Sun, J. Clavilier, A. Bewick, The mechanism of electrocatalytic oxidation of formic acid on Pt (100) and Pt (111) in sulphuric acid solution: an emirs study, *J. Electroanal. Chem. Interfacial Electrochem.* 240 (1988) 147-159.

[33] J.H. Jiang, J. Scott, A. Wieckowski, Direct evidence of a triple-path mechanism of formate electrooxidation on Pt black in alkaline media at varying temperature. Part I: The electrochemical studies, *Electrochimica Acta* 104 (2013) 124-133.

[34] P.A. Christensen, A. Hamnett, D. Linares-Moya, The electro-oxidation of formate ions at a polycrystalline Pt electrode in alkaline solution: an in situ FTIR study, *Phys. Chem. Chem. Phys.* 13 (2011) 11739-11747.

[35] B.A.F. Previdello, E.G. Machado, H. Varela, The effect of the alkali metal cation

on the electrocatalytic oxidation of formate on platinum, *RSC Adv.* 4 (2014) 15271-15275.

[36] M. Rosenbaum, U. Schröder, F. Scholz, Investigation of the electrocatalytic oxidation of formate and ethanol at platinum black under microbial fuel cell conditions, *J. Solid State Electrochem.* 10 (2006) 872-878.

[37] K. Ohyama, C. Kimura, H. Aoki, S. Kuwabata, T. Sugino, Evaluation of solid ammonium formate oxidation for polymer electrolyte fuel cells, *ECS Transactions* 11 (2007) 1473-1477.

[38] K. Ohyama, T. Sugino, T. Nitta, C. Kimura, H. Aoki, Improvement of anode oxidation reaction of a fuel cell using ammonium formate with Pt-Ir catalysis, *Electrical Engineering in Japan* 174 (2011) 1600-1604.

[39] H. Aoki, T. Nitta, S. Kuwabata, C. Kimura, T. Sugino, Improvement of anodic oxidation reaction of a fuel cell using ammonium formate with Pt-Pd catalysts, *ECS Transactions* 16 (2008) 849-853.

[40] A.M. Bartrom, G. Ognibene, J. Ta, J. Tran, J.L. Haan, Catalysts for alkaline direct ethanol and direct formate fuel cells, *ECS Transactions* 50 (2012) 1913-1918.

[41] J. Noborikawa, J. Lau, J. Ta, S. Hu, L. Scudiero, S. Derakhsha, S. Ha, J.L. Haan, Palladium-copper electrocatalyst for promotion of oxidation of formate and ethanol in alkaline media, *Electrochimica Acta* 137 (2014) 654-660.

- [42] S.G. da Silva, J.C.M. Silva, G.S. Buzzo, E.V. Spinacé, A.O. Neto, M.H.M.T. Assumpção, PdAu/C electrocatalysts as anodes for direct formate fuel cell, *Electrocatalysis* 6 (2015) 442-446.
- [43] F. Munoz, C. Hua, T. Kwong, L. Tran, T.Q. Nguyen, J.L. Haan, Palladium-copper electrocatalyst for the promotion of the electrochemical oxidation of polyalcohol fuels in the alkaline direct alcohol fuel cell, *Applied Catalysis B: Environmental* 174-175 (2015) 323-328.
- [44] C. Bianchini, P.K. Shen, Palladium-based electrocatalysts for alcohol oxidation in half cells and in direct alcohol fuel cells, *Chem. Rev.* 109 (2009) 4183-4206.
- [45] J.R. Varcoe, R.C.T. Slade, Prospects for alkaline anion-exchange membranes in low temperature fuel cells, *Fuel Cells* 5 (2005) 187-200.
- [46] L. An, T.S. Zhao, X.H. Yan, X.L. Zhou, P. Tan, The dual role of hydrogen peroxide in fuel cells, *Science Bulletin* 60 (2015) 55-64.
- [47] L. An, Z.H. Chai, L. Zeng, P. Tan, T.S. Zhao, Mathematical modeling of alkaline direct ethanol fuel cells, *Int. J. Hydrogen Energy* 38 (2013) 14067 -14075.
- [48] J.H. Jiang, A. Wieckowski, Prospective direct formate fuel cell, *Electrochemistry Communications* 18 (2012) 41-43.
- [49] T.Q. Nguyen, A.M. Bartrom, K. Tran, J.L. Haan, Operation of the alkaline direct formate fuel cell in the absence of added hydroxide, *Fuel cells* 13 (2013) 922-926.

- [50] A.M. Bartrom, J.L. Haan, The direct formate fuel cell with an alkaline anion exchange membrane, *Journal of Power Sources* 214 (2012) 68-74.
- [51] US 2013/0236809 A1, Direct formate fuel cell employing formate salt fuel, an anion exchange membrane, and metal catalysts, Sep. 12, 2013.
- [52] A.M. Bartrom, J. Ta, T.Q. Nguyen, J. Her, A. Donovan, J.L. Haan, Optimization of an anode fabrication method for the alkaline direct formate fuel cell, *Journal of Power Sources* 229 (2013) 234-238.
- [53] K. Tran, T.Q. Nguyen, A.M. Bartrom, A. Sadiki, J.L. Haan, A fuel-flexible alkaline direct liquid fuel cell, *Fuel Cells* 14 (2014) 834-841.
- [54] T.Q. Nguyen, D. Minami, C. Hua, A. Miller, K. Tran, J.L. Haan, Ambient temperature operation of a platinum-free direct formate fuel cell, *Journal of Fuel Cell Science and Technology* 12 (2015) 1-4.
- [55] L. Zeng, Z.K. Tang, T.S. Zhao, A high-performance alkaline exchange membrane direct formate fuel cell, *Applied Energy* 115 (2014) 405-410.
- [56] Y.S. Li, H. Wu, Y.L. He, Y. Liu, L. Jin, Performance of direct formate-peroxide fuel cells, *Journal of Power Sources* 287 (2015) 75-80.
- [57] Y.S. Li, A liquid-electrolyte-free anion-exchange membrane direct formate-peroxide fuel cell, *Int. J. Hydrogen Energy* 41 (2016) 3600-3604.
- [58] X.W. Yu, A. Manthiram, MnNiCoO<sub>4</sub>/N-MWCNT nanocomposite catalyst with

high selectivity in membraneless direct formate fuel cells and bifunctional activity for oxygen electrochemistry, *Catal. Sci. Technol.* 5 (2015) 2072-2075.

[59] T.S. Copenhaver, K.H. Purohit, K. Domalaon, L. Pham, B.J. Burgess, N. Manorohtkul, V. Galvan, S. Sotez, F.A. Gomez, J.L. Haan, A microfluidic direct formate fuel cell on paper, *Electrophoresis* 36 (2015) 1825-1829.

[60] V. Galvan, K. Domalaon, G. Tang, S. Sotez, A. Mendez, M. Jalali-Heravi, K. Purohit, L. Pham, J. Haan, F.A. Gomez, An improved alkaline direct formate paper microfluidic fuel cell, *Electrophoresis* 37 (2016) 504-510.

[61] L. An, T.S. Zhao, R. Chen, Q.X. Wu, A novel direct ethanol fuel cell with high power density, *J. Power Sources* 196 (2011) 6219–6222.

[62] L. An, T.S. Zhao, Z.H. Chai, L. Zeng, P. Tan, Modeling of the mixed potential in hydrogen peroxide-based fuel cells, *Int. J. Hydrogen Energy* 39 (2014) 7407-7416.

[63] X.L. Zhou, T.S. Zhao, L. An, L. Wei, C. Zhang, The use of polybenzimidazole membranes in vanadium redox flow batteries leading to increased coulombic efficiency and cycling performance, *Electrochimica Acta* 153 (2015) 492–498.

[64] T. Reda, C.M. Plugge, N.J. Abram, J. Hirst, Reversible interconversion of carbon dioxide and formate by an electroactive enzyme, *PNAS* 105 (2008) 10654-10658.

[65] A.S. Agarwal, Y. Zhai, D. Hill, N. Sridhar, The electrochemical reduction of carbon dioxide to formate/formic acid: engineering and economic feasibility,

ChemSusChem 4 (2011) 1301-1310.

[66] T. Arai, S. Tajima, S. Sato, K. Uemura, T. Morikawa, T. Kajino, Selective CO<sub>2</sub> conversion to formate in water using a CZTS photocathode modified with a ruthenium complex polymer, Chem. Commun. 47 (2011) 12664-12666.

**Table captions:**

Table 1 Exchange current densities of formate oxidation measured in different electrolyte compositions at 20°C and 45°C [30].

Table 2 The DFFC performance at 60°C in the literature.

Table 3 The DFFC performance at other temperatures in the literature.

**Figure captions:**

Fig. 1 Schematic of a direct formate fuel cell (DFFC).

Fig. 2 (a) Current densities for various catalysts (Pt-Pd, Pt-Ir, Pt-Ru, Pt) in 0.1 M HCOONH<sub>4</sub> at 0 V of CVs [39] and (b) proposed mechanism for the formate oxidation on Pt [31].

Fig. 3 The DFFC performance evaluation: (a) voltage/power-current curves and (b) constant-current discharging behaviors [49].

Fig. 4 The DFFC performance improvements through optimizing (a) the operating

parameters [50] and (b) the structural design parameters [52]; and (c) performance comparison among fuel cells running on various fuels (formate, ethanol, ethylene glycol) [52].

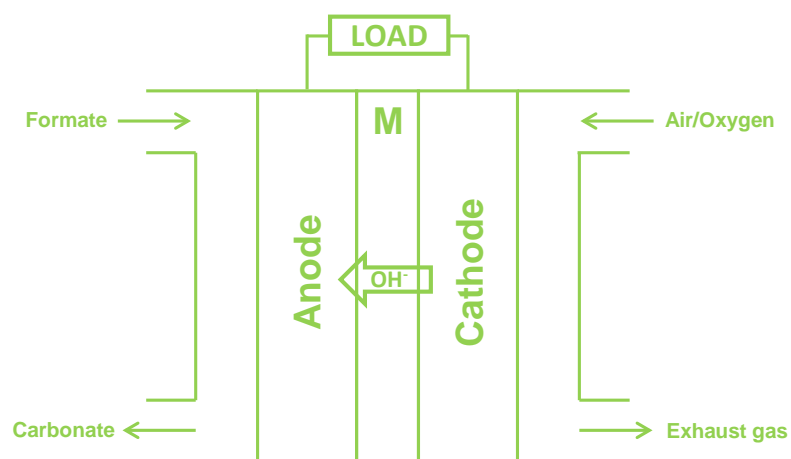
Fig. 5 A formate-hydrogen peroxide fuel cell: (a) schematic [13] and (b) performance [56]. A membraneless formate fuel cell: (c) schematic and (d) performance [15].

Fig. 6 A microfluidic formate fuel cell with flow-through porous electrodes: (a) schematic, (b) image of the assembled cell with porous palladium and gold electrodes, and (c) the labeled image of the assembled cell [16].

Fig. 7 A microfluidic formate fuel cell on paper: (a) Y-shaped design [59] and (b) demos (three light-emitting diodes and a handheld calculator) [60].

Fig. 8 An electrochemical energy-storage system using formate as energy carrier: (a) schematic and (b) working principle [61].

**Graphical Abstract:** This article provides a review of past research on the development of this type of fuel cell, including the working principle, mechanisms and materials of the electrocatalytic oxidation of formate, single-cell designs and performance, as well as innovative system designs.



### Highlights

- This article reviews past research on the development of direct formate fuel cells.
- Particular attention is paid to mechanisms and materials of formate oxidation.
- Single-cell designs and their performance are summarized and discussed.
- Innovative system designs and future perspectives are highlighted.

Electrolyte composition	T (°C)	$i_0$ (mA cm <sup>-2</sup> )
1 M KOH + 0.5 M KCOOH	20	0.64
	45	1.00
1 M KOH + 0.5 M KCOOH + 2 M K <sub>2</sub> CO <sub>3</sub>	20	0.85
	45	1.40
1 M KOH + 0.5 M KCOOH + 1 M K <sub>2</sub> CO <sub>3</sub>	20	1.07

	45	1.75
	20	0.26

Fuel/Oxidant	Anode	Cathode	Membrane	T (°C)	PPD (mW cm <sup>-2</sup> )	Ref.
--------------	-------	---------	----------	--------	----------------------------	------

1 M NaOH + 0.5 M NaCOOH

	45	0.71
1 M NaOH + 0.5 M NaCOOH + 2 M Na <sub>2</sub> CO <sub>3</sub>	20	0.64
	45	0.83
0.5 M KOH + 0.5 M NaOH + 0.25 M KCOOH + 0.25 M NaCOOH	20	0.36
	45	0.84
0.5 M KOH + 0.5 M NaOH + 0.25 M KCOOH + 0.25 M NaCOOH + 1 M K <sub>2</sub> CO <sub>3</sub> + 1 M Na <sub>2</sub> CO <sub>3</sub>	20	0.68
	45	1.06

Table 1 Exchange current densities of formate oxidation measured in different electrolyte compositions at 20°C and 45°C [30].

2 mL min <sup>-1</sup> 1 M HCOONa + 2 M NaOH / 10 mL min <sup>-1</sup> 1 M H <sub>2</sub> O <sub>2</sub> + 1 M H <sub>2</sub> SO <sub>4</sub>	PdAu/Ni foam (3 mg cm <sup>-2</sup> )	PdAu/Ni foam (3 mg cm <sup>-2</sup> )	Nafion 115 membrane	60	331	[13]
1 mL min <sup>-1</sup> 2 M HCOOK + 2 M KOH / 100 sccm O <sub>2</sub>	Pd/C (2 mg cm <sup>-2</sup> )	Pt/C (2 mg cm <sup>-2</sup> )	Tokuyama A201 membrane	60	144	[40]
1 mL min <sup>-1</sup> 2 M HCOOK + 2 M KOH / 400 sccm air	Pd/C (2 mg cm <sup>-2</sup> )	Pt/C (2 mg cm <sup>-2</sup> )	Tokuyama A201 membrane	60	109	[40]
1 mL min <sup>-1</sup> 2 M HCOOK / 100 sccm O <sub>2</sub>	Pd/C (2 mg cm <sup>-2</sup> )	Pt/C (2 mg cm <sup>-2</sup> )	Tokuyama A201 membrane	60	51	[40]
1 mL min <sup>-1</sup> 2 M HCOOK + 2M NaOH / 100 sccm O <sub>2</sub>	Pd/C (2 mg cm <sup>-2</sup> )	Pt/C (2 mg cm <sup>-2</sup> )	Tokuyama A201 membrane	60	125	[40]
1 mL min <sup>-1</sup> 1 M HCOONa + 2 M KOH / 150 sccm O <sub>2</sub>	Au/C (2 mg cm <sup>-2</sup> )	Pt/C (2 mg cm <sup>-2</sup> )	Nafion 117 membrane	60	2.1	[42]
1 mL min <sup>-1</sup> 1 M HCOONa + 2 M KOH / 150 sccm O <sub>2</sub>	PdAu/C 50:50 (2 mg cm <sup>-2</sup> )	Pt/C (2 mg cm <sup>-2</sup> )	Nafion 117 membrane	60	12.3	[42]
1 mL min <sup>-1</sup> 1 M HCOONa + 2 M KOH / 150 sccm O <sub>2</sub>	PdAu/C 70:30 (2 mg cm <sup>-2</sup> )	Pt/C (2 mg cm <sup>-2</sup> )	Nafion 117 membrane	60	12.7	[42]
1 mL min <sup>-1</sup> 1 M HCOONa + 2 M KOH / 150 sccm O <sub>2</sub>	PdAu/C 80:20 (2 mg cm <sup>-2</sup> )	Pt/C (2 mg cm <sup>-2</sup> )	Nafion 117 membrane	60	13.8	[42]
1 mL min <sup>-1</sup> 1 M HCOONa + 2 M KOH / 150 sccm O <sub>2</sub>	PdAu/C 90:10 (2 mg cm <sup>-2</sup> )	Pt/C (2 mg cm <sup>-2</sup> )	Nafion 117 membrane	60	14.0	[42]
1 mL min <sup>-1</sup> 1 M HCOONa + 2 M KOH / 150 sccm O <sub>2</sub>	Pd/C (2 mg cm <sup>-2</sup> )	Pt/C (2 mg cm <sup>-2</sup> )	Nafion 117 membrane	60	12.6	[42]
1 mL min <sup>-1</sup> 1 M HCOOK + 2 M KOH / 100 sccm O <sub>2</sub>	Pd/C (2 mg cm <sup>-2</sup> )	Pt/C (2 mg cm <sup>-2</sup> )	Tokuyama A201 membrane	60	144	[50]
1 mL min <sup>-1</sup> 1 M HCOOK + 1 M KOH / 100 sccm O <sub>2</sub>	Pd/C (2 mg cm <sup>-2</sup> )	Pt/C (2 mg cm <sup>-2</sup> )	Tokuyama A201 membrane	60	125	[50]
1 mL min <sup>-1</sup> 1 M HCOOK / 100 sccm O <sub>2</sub>	Pd/C (2 mg cm <sup>-2</sup> )	Pt/C (2 mg cm <sup>-2</sup> )	Tokuyama A201 membrane	60	51	[50]
1 mL min <sup>-1</sup> 2 M HCOOK + 2 M KOH / 100 sccm O <sub>2</sub>	Pd/C (2 mg cm <sup>-2</sup> )	Pt/C (2 mg cm <sup>-2</sup> )	Tokuyama A201 membrane	60	~123	[50]
1 mL min <sup>-1</sup> 3 M HCOOK + 2 M KOH / 100 sccm O <sub>2</sub>	Pd/C (2 mg cm <sup>-2</sup> )	Pt/C (2 mg cm <sup>-2</sup> )	Tokuyama A201 membrane	60	~77	[50]
1 mL min <sup>-1</sup> 1 M HCOONa + 2 M KOH / 100 sccm O <sub>2</sub>	Pd/C (2 mg cm <sup>-2</sup> )	Pt/C (2 mg cm <sup>-2</sup> )	Tokuyama A201 membrane	60	125	[50]
1 mL min <sup>-1</sup> 1 M HCOOK + 2 M KOH / 400 sccm air	Pd/C (2 mg cm <sup>-2</sup> )	Pt/C (2 mg cm <sup>-2</sup> )	Tokuyama A201 membrane	60	~110	[50]
1 mL min <sup>-1</sup> 2 M HCOOK + 2 M KOH / 100 sccm O <sub>2</sub>	Pd/C (2 mg cm <sup>-2</sup> )	Pt/C (2 mg cm <sup>-2</sup> )	Tokuyama A201 membrane	60	61	[50]

M KOH / 100 sccm O <sub>2</sub>						
1 mL min <sup>-1</sup> 1 M HCOOK + 2 M KOH / 100 sccm O <sub>2</sub>	Pd/C (4 mg cm <sup>-2</sup> ) via spray painted on the membrane	Pt/C (4 mg cm <sup>-2</sup> ) via brush painted on the GDL	Tokuyama A201 membrane	60	267	[52]
1 mL min <sup>-1</sup> 1 M HCOOK / 100 sccm O <sub>2</sub>	Pd/C (4 mg cm <sup>-2</sup> ) via spray painted on the membrane	Pt/C (4 mg cm <sup>-2</sup> ) via brush painted on the GDL	Tokuyama A201 membrane	60	157	[52]
1 mL min <sup>-1</sup> 1 M HCOOK + 2 M KOH / 400 sccm air	Pd/C (4 mg cm <sup>-2</sup> ) via spray painted on the membrane	Pt/C (4 mg cm <sup>-2</sup> ) via brush painted on the GDL	Tokuyama A201 membrane	60	167	[52]
1 mL min <sup>-1</sup> 1 M HCOOK / 400 sccm air	Pd/C (4 mg cm <sup>-2</sup> ) via spray painted on the membrane	Pt/C (4 mg cm <sup>-2</sup> ) via brush painted on the GDL	Tokuyama A201 membrane	60	105	[52]
1 mL min <sup>-1</sup> 1 M HCOOK + 2 M KOH / 100 sccm O <sub>2</sub>	Pd/C (4 mg cm <sup>-2</sup> ) 2 mg cm <sup>-2</sup> via direct painted on membrane and 2 mg cm <sup>-2</sup> via painted on carbon cloth	Pt/C (2 mg cm <sup>-2</sup> ) via direct painted on membrane	Tokuyama A201 membrane	60	302	[53]
1 mL min <sup>-1</sup> 1 M HCOOK / 400 sccm air	Pd/C (4 mg cm <sup>-2</sup> ) 2 mg cm <sup>-2</sup> via direct painted on membrane and 2 mg cm <sup>-2</sup> via painted on carbon cloth	Pt/C (2 mg cm <sup>-2</sup> ) via direct painted on membrane	Tokuyama A201 membrane	60	120	[53]
2 mL min <sup>-1</sup> 1 M HCOOK + 2 M KOH / 100 sccm O <sub>2</sub>	Pd/C (2 mg cm <sup>-2</sup> )	Fe-Co HYPERMEC™ K14 (2 mg cm <sup>-2</sup> )	QAPSF membrane	60	~110	[55]
2 mL min <sup>-1</sup> 1 M HCOOK + 1 M KOH / 100 sccm O <sub>2</sub>	Pd/C (2 mg cm <sup>-2</sup> )	Fe-Co HYPERMEC™ K14 (2 mg cm <sup>-2</sup> )	QAPSF membrane	60	~110	[55]
2 mL min <sup>-1</sup> 1 M HCOOK + 0.5 M KOH / 100 sccm O <sub>2</sub>	Pd/C (2 mg cm <sup>-2</sup> )	Fe-Co HYPERMEC™ K14 (2 mg cm <sup>-2</sup> )	QAPSF membrane	60	~94	[55]
2 mL min <sup>-1</sup> 1 M HCOOK / 100 sccm O <sub>2</sub>	Pd/C (2 mg cm <sup>-2</sup> )	Fe-Co HYPERMEC™ K14 (2 mg cm <sup>-2</sup> )	QAPSF membrane	60	~40	[55]
2 mL min <sup>-1</sup> 2 M HCOOK + 1 M KOH / 100 sccm O <sub>2</sub>	Pd/C (2 mg cm <sup>-2</sup> )	Fe-Co HYPERMEC™ K14 (2 mg cm <sup>-2</sup> )	QAPSF membrane	60	~125	[55]
2 mL min <sup>-1</sup> 3 M HCOOK + 1 M KOH / 100 sccm O <sub>2</sub>	Pd/C (2 mg cm <sup>-2</sup> )	Fe-Co HYPERMEC™ K14 (2 mg cm <sup>-2</sup> )	QAPSF membrane	60	~150	[55]
2 mL min <sup>-1</sup> 5 M HCOOK + 1	Pd/C (2 mg cm <sup>-2</sup> )	Fe-Co HYPERMEC™	QAPSF membrane	60	~165	[55]

M KOH / 100 sccm O <sub>2</sub>		K14 (2 mg cm <sup>-2</sup> )				
2 mL min <sup>-1</sup> 7 M HCOOK + 1 M KOH / 100 sccm O <sub>2</sub>	Pd/C (2 mg cm <sup>-2</sup> )	Fe-Co HYPERMEC™ K14 (2 mg cm <sup>-2</sup> )	QAPSF membrane	60	~175	[55]
2 mL min <sup>-1</sup> 1 M HCOONa + 2 M NaOH / 10 mL min <sup>-1</sup> 1 M H <sub>2</sub> O <sub>2</sub> + 1 M H <sub>2</sub> SO <sub>4</sub>	Pd/C (1 mg cm <sup>-2</sup> )	Pt/C (2 mg cm <sup>-2</sup> )	Nafion 115 membrane	60	407	[56]
2 mL min <sup>-1</sup> 1 M HCOONa + 2 M NaOH / 10 mL min <sup>-1</sup> 1 M H <sub>2</sub> O <sub>2</sub> + 1 M H <sub>2</sub> SO <sub>4</sub>	Pd/C (2 mg cm <sup>-2</sup> )	Pt/C (2 mg cm <sup>-2</sup> )	Nafion 115 membrane	60	442	[56]
2 mL min <sup>-1</sup> 1 M HCOONa + 2 M NaOH / 10 mL min <sup>-1</sup> 1 M H <sub>2</sub> O <sub>2</sub> + 1 M H <sub>2</sub> SO <sub>4</sub>	Pd/C (3 mg cm <sup>-2</sup> )	Pt/C (2 mg cm <sup>-2</sup> )	Nafion 115 membrane	60	~380	[56]
2 mL min <sup>-1</sup> 1 M HCOONa + 2 M NaOH / 10 mL min <sup>-1</sup> 1 M H <sub>2</sub> O <sub>2</sub> + 1 M H <sub>2</sub> SO <sub>4</sub>	Pd/C (4 mg cm <sup>-2</sup> )	Pt/C (2 mg cm <sup>-2</sup> )	Nafion 115 membrane	60	341	[56]
2 mL min <sup>-1</sup> 1 M HCOONa + 2 M NaOH / 10 mL min <sup>-1</sup> 1 M H <sub>2</sub> O <sub>2</sub> + 1 M H <sub>2</sub> SO <sub>4</sub>	Pd/C (2 mg cm <sup>-2</sup> )	Pt/C (1 mg cm <sup>-2</sup> )	Nafion 115 membrane	60	412	[56]
2 mL min <sup>-1</sup> 1 M HCOONa + 2 M NaOH / 10 mL min <sup>-1</sup> 1 M H <sub>2</sub> O <sub>2</sub> + 1 M H <sub>2</sub> SO <sub>4</sub>	Pd/C (2 mg cm <sup>-2</sup> )	Pt/C (3 mg cm <sup>-2</sup> )	Nafion 115 membrane	60	~400	[56]
2 mL min <sup>-1</sup> 1 M HCOONa + 2 M NaOH / 10 mL min <sup>-1</sup> 1 M H <sub>2</sub> O <sub>2</sub> + 1 M H <sub>2</sub> SO <sub>4</sub>	Pd/C (2 mg cm <sup>-2</sup> )	Pt/C (4 mg cm <sup>-2</sup> )	Nafion 115 membrane	60	367	[56]
2 mL min <sup>-1</sup> 0.5 M HCOONa + 2 M NaOH / 10 mL min <sup>-1</sup> 1 M H <sub>2</sub> O <sub>2</sub> + 1 M H <sub>2</sub> SO <sub>4</sub>	Pd/C (2 mg cm <sup>-2</sup> )	Pt/C (2 mg cm <sup>-2</sup> )	Nafion 115 membrane	60	485	[56]
2 mL min <sup>-1</sup> 1 M HCOONa + 2 M NaOH / 10 mL min <sup>-1</sup> 1 M H <sub>2</sub> O <sub>2</sub> + 1 M H <sub>2</sub> SO <sub>4</sub>	Pd/C (2 mg cm <sup>-2</sup> )	Pt/C (2 mg cm <sup>-2</sup> )	Nafion 115 membrane	60	519	[56]
2 mL min <sup>-1</sup> 2 M HCOONa + 2 M NaOH / 10 mL min <sup>-1</sup> 1 M H <sub>2</sub> O <sub>2</sub> + 1 M H <sub>2</sub> SO <sub>4</sub>	Pd/C (2 mg cm <sup>-2</sup> )	Pt/C (2 mg cm <sup>-2</sup> )	Nafion 115 membrane	60	~492	[56]
2 mL min <sup>-1</sup> 3 M HCOONa + 2 M NaOH / 10 mL min <sup>-1</sup> 1 M H <sub>2</sub> O <sub>2</sub> + 1 M H <sub>2</sub> SO <sub>4</sub>	Pd/C (2 mg cm <sup>-2</sup> )	Pt/C (2 mg cm <sup>-2</sup> )	Nafion 115 membrane	60	477	[56]
2 mL min <sup>-1</sup> 1 M HCOONa + 1 M NaOH / 10 mL min <sup>-1</sup> 1 M	Pd/C (2 mg cm <sup>-2</sup> )	Pt/C (2 mg cm <sup>-2</sup> )	Nafion 115 membrane	60	~430	[56]

H <sub>2</sub> O <sub>2</sub> + 1 M H <sub>2</sub> SO <sub>4</sub>						
2 mL min <sup>-1</sup> 1 M HCOONa + 3 M NaOH / 10 mL min <sup>-1</sup> 1 M H <sub>2</sub> O <sub>2</sub> + 1 M H <sub>2</sub> SO <sub>4</sub>	Pd/C (2 mg cm <sup>-2</sup> )	Pt/C (2 mg cm <sup>-2</sup> )	Nafion 115 membrane	60	591	[56]
2 mL min <sup>-1</sup> 1 M HCOONa + 4 M NaOH / 10 mL min <sup>-1</sup> 1 M H <sub>2</sub> O <sub>2</sub> + 1 M H <sub>2</sub> SO <sub>4</sub>	Pd/C (2 mg cm <sup>-2</sup> )	Pt/C (2 mg cm <sup>-2</sup> )	Nafion 115 membrane	60	~550	[56]
2 mL min <sup>-1</sup> 1 M HCOONa + 6 M NaOH / 10 mL min <sup>-1</sup> 1 M H <sub>2</sub> O <sub>2</sub> + 1 M H <sub>2</sub> SO <sub>4</sub>	Pd/C (2 mg cm <sup>-2</sup> )	Pt/C (2 mg cm <sup>-2</sup> )	Nafion 115 membrane	60	~520	[56]
2 mL min <sup>-1</sup> 1 M HCOONa + 1 M NaOH / 10 mL min <sup>-1</sup> 8 M H <sub>2</sub> O <sub>2</sub> + 1 M H <sub>2</sub> SO <sub>4</sub>	Pd/C (2 mg cm <sup>-2</sup> )	Pt/C (2 mg cm <sup>-2</sup> )	Nafion 115 membrane	60	~410	[56]
<b>Fuel/Oxidant</b>	<b>Anode</b>	<b>Cathode</b>	<b>Membrane</b>	<b>T (°C)</b>	<b>PPD (mW cm<sup>-2</sup>)</b>	<b>Ref.</b>

Table 2 The DFFC performance at 60°C in the literature.

60 $\mu\text{L min}^{-1}$ 1.2 M HCOONa / 60 $\mu\text{L min}^{-1}$ 0.67 M hypochlorite	Pd/C (5 mg $\text{cm}^{-2}$ )	Au/C (5 mg $\text{cm}^{-2}$ )	Membraneless	R.T.	52	[16]
10 $\mu\text{L min}^{-1}$ 1.2 M HCOONa / 60 $\mu\text{L min}^{-1}$ 0.67 M hypochlorite	Pd/C (5 mg $\text{cm}^{-2}$ )	Au/C (5 mg $\text{cm}^{-2}$ )	Membraneless	R.T.	~32	[16]
2 $\mu\text{L min}^{-1}$ 1.2 M HCOONa / 60 $\mu\text{L min}^{-1}$ 0.67 M hypochlorite	Pd/C (5 mg $\text{cm}^{-2}$ )	Au/C (5 mg $\text{cm}^{-2}$ )	Membraneless	R.T.	18	[16]
0.5 M HCOONa / ambient air	Pd/AS-4 quaternary ammonium ionomer (Tokuyama) (3 mg $\text{cm}^{-2}$ )	Pt/AS-4 quaternary ammonium ionomer (Tokuyama) (3 mg $\text{cm}^{-2}$ )	Tokuyama A201 membrane	R.T.	2.5	[22]
2 mL $\text{min}^{-1}$ 1 M HCOOK / 100 sccm $\text{O}_2$	Pd/C (2 mg $\text{cm}^{-2}$ )	Pt/C (4 mg $\text{cm}^{-2}$ )	Tokuyama A201 membrane	R.T.	64	[33]
2 mL $\text{min}^{-1}$ 1 M HCOOK / 400 sccm air	Pd/C (2 mg $\text{cm}^{-2}$ )	Pt/C (4 mg $\text{cm}^{-2}$ )	Tokuyama A201 membrane	R.T.	27	[33]
1 mL $\text{min}^{-1}$ 1 M HCOOK + 2 M KOH / 400 sccm air	Pd/C (2 mg $\text{cm}^{-2}$ )	ACTA HYPERMEC™ 4020 Fe-Co (0.75 mg $\text{cm}^{-2}$ )	Tokuyama A201 membrane	20	35	[54]
1 mL $\text{min}^{-1}$ 1 M HCOOK + 2 M KOH / 100 sccm $\text{O}_2$	Pd/C (2 mg $\text{cm}^{-2}$ )	ACTA HYPERMEC™ 4020 Fe-Co (0.75 mg $\text{cm}^{-2}$ )	Tokuyama A201 membrane	20	45	[54]
1 mL $\text{min}^{-1}$ 1 M HCOOK / 100 sccm $\text{O}_2$	Pd/C (2 mg $\text{cm}^{-2}$ )	ACTA HYPERMEC™ 4020 Fe-Co (0.75 mg $\text{cm}^{-2}$ )	Tokuyama A201 membrane	20	18	[54]
2 mL $\text{min}^{-1}$ 1 M HCOONa + 2 M NaOH / 10 mL $\text{min}^{-1}$ 1 M $\text{H}_2\text{O}_2$ + 1 M $\text{H}_2\text{SO}_4$	PdAu/Ni foam (3 mg $\text{cm}^{-2}$ )	PdAu/Ni foam (3 mg $\text{cm}^{-2}$ )	Nafion 115 membrane	25	214	[19]
2 mL $\text{min}^{-1}$ 1 M HCOONa + 3 M NaOH / 10 mL $\text{min}^{-1}$ 8 M $\text{H}_2\text{O}_2$ + 1 M $\text{H}_2\text{SO}_4$	Pd/C (2 mg $\text{cm}^{-2}$ )	Pt/C (2 mg $\text{cm}^{-2}$ )	Nafion 115 membrane	25	~310	[56]
2 mL $\text{min}^{-1}$ 1 M HCOOK / 100 sccm $\text{O}_2$	Pd/C (2 mg $\text{cm}^{-2}$ )	Pt/C (4 mg $\text{cm}^{-2}$ )	Tokuyama A201 membrane	30	~78	[33]
2 mL $\text{min}^{-1}$ 1 M HCOOK / 400 sccm air	Pd/C (2 mg $\text{cm}^{-2}$ )	Pt/C (4 mg $\text{cm}^{-2}$ )	Tokuyama A201 membrane	30	~40	[33]
1 mL $\text{min}^{-1}$ 1 M HCOOK + 2 M KOH / 100 sccm $\text{O}_2$	Pd/C (2 mg $\text{cm}^{-2}$ )	ACTA HYPERMEC™ 4020 Fe-Co	Tokuyama A201 membrane	30	~65	[54]

		(0.75 mg cm <sup>-2</sup> )				
1 mL min <sup>-1</sup> 1 M HCOOK + 2 M KOH / 400 sccm air	Pd/C (2 mg cm <sup>-2</sup> )	ACTA HYPERMEC™ 4020 Fe-Co (0.75 mg cm <sup>-2</sup> )	Tokuyama A201 membrane	30	~44	[54]
1 mL min <sup>-1</sup> 1 M HCOOK / 100 sccm O <sub>2</sub>	Pd/C (2 mg cm <sup>-2</sup> )	ACTA HYPERMEC™ 4020 Fe-Co (0.75 mg cm <sup>-2</sup> )	Tokuyama A201 membrane	30	~22	[54]
2 mL min <sup>-1</sup> 1 M HCOONa + 3 M NaOH / 10 mL min <sup>-1</sup> 8 M H <sub>2</sub> O <sub>2</sub> + 1 M H <sub>2</sub> SO <sub>4</sub>	Pd/C (2 mg cm <sup>-2</sup> )	Pt/C (2 mg cm <sup>-2</sup> )	Nafion 115 membrane	30	~350	[56]
1 mL min <sup>-1</sup> 1 M HCOOK + 2 M KOH / 100 sccm O <sub>2</sub>	Pd/C (4 mg cm <sup>-2</sup> ) via spray painted on the membrane	Pt/C (4 mg cm <sup>-2</sup> ) via brush painted on the GDL	Tokuyama A201 membrane	35	141	[52]
2 mL min <sup>-1</sup> 1 M HCOONa + 2 M NaOH / 10 mL min <sup>-1</sup> 1 M H <sub>2</sub> O <sub>2</sub> + 1 M H <sub>2</sub> SO <sub>4</sub>	PdAu/Ni foam (3 mg cm <sup>-2</sup> )	PdAu/Ni foam (3 mg cm <sup>-2</sup> )	Nafion 115 membrane	40	~250	[13]
2 mL min <sup>-1</sup> 1 M HCOOK / 100 sccm O <sub>2</sub>	Pd/C (2 mg cm <sup>-2</sup> )	Pt/C (4 mg cm <sup>-2</sup> )	Tokuyama A201 membrane	40	~87	[33]
2 mL min <sup>-1</sup> 1 M HCOOK / 400 sccm air	Pd/C (2 mg cm <sup>-2</sup> )	Pt/C (4 mg cm <sup>-2</sup> )	Tokuyama A201 membrane	40	~64	[33]
1 mL min <sup>-1</sup> 1 M HCOOK + 2 M KOH / 100 sccm O <sub>2</sub>	Pd/C (2 mg cm <sup>-2</sup> )	Pt/C (2 mg cm <sup>-2</sup> )	Tokuyama A201 membrane	40	107	[50]
1 mL min <sup>-1</sup> 1 M HCOOK + 2 M KOH / 100 sccm O <sub>2</sub>	Pd/C (2 mg cm <sup>-2</sup> )	ACTA HYPERMEC™ 4020 Fe-Co (0.75 mg cm <sup>-2</sup> )	Tokuyama A201 membrane	40	~78	[54]
1 mL min <sup>-1</sup> 1 M HCOOK + 2 M KOH / 400 sccm air	Pd/C (2 mg cm <sup>-2</sup> )	ACTA HYPERMEC™ 4020 Fe-Co (0.75 mg cm <sup>-2</sup> )	Tokuyama A201 membrane	40	~51	[54]
1 mL min <sup>-1</sup> 1 M HCOOK / 100 sccm O <sub>2</sub>	Pd/C (2 mg cm <sup>-2</sup> )	ACTA HYPERMEC™ 4020 Fe-Co (0.75 mg cm <sup>-2</sup> )	Tokuyama A201 membrane	40	~25	[54]
2 mL min <sup>-1</sup> 1 M HCOONa + 3 M NaOH / 10 mL min <sup>-1</sup> 8 M H <sub>2</sub> O <sub>2</sub> + 1 M H <sub>2</sub> SO <sub>4</sub>	Pd/C (2 mg cm <sup>-2</sup> )	Pt/C (2 mg cm <sup>-2</sup> )	Nafion 115 membrane	40	~420	[56]
1 mL min <sup>-1</sup> 1 M HCOOK / 3 mL min <sup>-1</sup> 15% H <sub>2</sub> O <sub>2</sub>	Pd/C (2 mg cm <sup>-2</sup> )	Pt/C (2 mg cm <sup>-2</sup> )	Tokuyama A201 membrane	40	23	[57]
1 mL min <sup>-1</sup> 3 M HCOOK / 3 mL min <sup>-1</sup> 15% H <sub>2</sub> O <sub>2</sub>	Pd/C (2 mg cm <sup>-2</sup> )	Pt/C (2 mg cm <sup>-2</sup> )	Tokuyama A201 membrane	40	~28	[57]

1 mL min <sup>-1</sup> 5 M HCOOK / 3 mL min <sup>-1</sup> 15% H <sub>2</sub> O <sub>2</sub>	Pd/C (2 mg cm <sup>-2</sup> )	Pt/C (2 mg cm <sup>-2</sup> )	Tokuyama A201 membrane	40	~31	[57]
1 mL min <sup>-1</sup> 7 M HCOOK / 3 mL min <sup>-1</sup> 15% H <sub>2</sub> O <sub>2</sub>	Pd/C (2 mg cm <sup>-2</sup> )	Pt/C (2 mg cm <sup>-2</sup> )	Tokuyama A201 membrane	40	~37	[57]
1 mL min <sup>-1</sup> 1 M HCOOK + 2 M KOH / 100 sccm O <sub>2</sub>	Pd/C (4 mg cm <sup>-2</sup> ) via spray painted on the membrane	Pt/C (4 mg cm <sup>-2</sup> ) via brush painted on the GDL	Tokuyama A201 membrane	45	185	[52]
2 mL min <sup>-1</sup> 1 M HCOONa + 2 M NaOH / 10 mL min <sup>-1</sup> 1 M H <sub>2</sub> O <sub>2</sub> + 1 M H <sub>2</sub> SO <sub>4</sub>	PdAu/Ni foam (3 mg cm <sup>-2</sup> )	PdAu/Ni foam (3 mg cm <sup>-2</sup> )	Nafion 115 membrane	50	~285	[13]
2 mL min <sup>-1</sup> 1 M HCOOK / 100 sccm O <sub>2</sub>	Pd/C (2 mg cm <sup>-2</sup> )	Pt/C (4 mg cm <sup>-2</sup> )	Tokuyama A201 membrane	50	106	[33]
2 mL min <sup>-1</sup> 1 M HCOOK / 400 sccm air	Pd/C (2 mg cm <sup>-2</sup> )	Pt/C (4 mg cm <sup>-2</sup> )	Tokuyama A201 membrane	50	76	[33]
1 mL min <sup>-1</sup> 1 M HCOOK + 2 M KOH / 100 sccm O <sub>2</sub>	Pd/C (2 mg cm <sup>-2</sup> )	ACTA HYPERMEC™ 4020 Fe-Co (0.75 mg cm <sup>-2</sup> )	Tokuyama A201 membrane	50	99	[54]
1 mL min <sup>-1</sup> 1 M HCOOK + 2 M KOH / 400 sccm air	Pd/C (2 mg cm <sup>-2</sup> )	ACTA HYPERMEC™ 4020 Fe-Co (0.75 mg cm <sup>-2</sup> )	Tokuyama A201 membrane	50	66	[54]
1 mL min <sup>-1</sup> 1 M HCOOK / 100 sccm O <sub>2</sub>	Pd/C (2 mg cm <sup>-2</sup> )	ACTA HYPERMEC™ 4020 Fe-Co (0.75 mg cm <sup>-2</sup> )	Tokuyama A201 membrane	50	27	[54]
2 mL min <sup>-1</sup> 1 M HCOONa + 3 M NaOH / 10 mL min <sup>-1</sup> 8 M H <sub>2</sub> O <sub>2</sub> + 1 M H <sub>2</sub> SO <sub>4</sub>	Pd/C (2 mg cm <sup>-2</sup> )	Pt/C (2 mg cm <sup>-2</sup> )	Nafion 115 membrane	50	~500	[56]
2 mL min <sup>-1</sup> 5 M HCOOK + 1 M KOH / 100 sccm O <sub>2</sub>	Pd/C (2 mg cm <sup>-2</sup> )	Fe-Co HYPERMEC™ K14 (2 mg cm <sup>-2</sup> )	QAPSF membrane	80	250	[55]
2 mL min <sup>-1</sup> 5 M HCOOK / 100 sccm O <sub>2</sub>	Pd/C (2 mg cm <sup>-2</sup> )	Fe-Co HYPERMEC™ K14 (2 mg cm <sup>-2</sup> )	QAPSF membrane	80	~125	[55]
6 mL min <sup>-1</sup> 2 M HCOOK + 2 M KOH / 200 sccm O <sub>2</sub>	Pd/C (4 mg cm <sup>-2</sup> )	Ag/C (8 mg cm <sup>-2</sup> )	Polybenzimidazole-based membrane (FuMA-Tech GmbH)	120	170	[48]
6 mL min <sup>-1</sup> 6 M HCOOK + 2 M KOH / 200 sccm O <sub>2</sub>	Pd/C (4 mg cm <sup>-2</sup> )	Ag/C (8 mg cm <sup>-2</sup> )	Polybenzimidazole-based membrane (FuMA-Tech GmbH)	120	160	[48]

Table 3 The DFFC performance at other temperatures in the literature.

